Boundary effects in the stepwise structure of the Lyapunov spectra for quasi-one-dimensional systems

Tooru Taniguchi and Gary P. Morriss
School of Physics, University of New South Wales, Sydney, New South Wales 2052, Australia
(Received 14 October 2002; published 26 August 2003)

Boundary effects in the stepwise structure of the Lyapunov spectra and corresponding wavelike structure of the Lyapunov vectors are discussed numerically in quasi-one-dimensional systems of many hard disks. Four different types of boundary conditions are constructed by combinations of periodic boundary conditions and hard-wall boundary conditions, and each leads to different stepwise structures of the Lyapunov spectra. We show that for some Lyapunov exponents in the step region, the spatial y component of the corresponding Lyapunov vector δq_{yj}, divided by the y component of momentum p_{yj}, exhibits a wavelike structure as a function of position q_{xj} and time t. For the other Lyapunov exponents in the step region, the y component of the corresponding Lyapunov vector δq_{yj} exhibits a time-independent wavelike structure as a function of q_{xj}. These two types of wavelike structure are used to categorize the type and sequence of steps in the Lyapunov spectra for each different type of boundary condition.

DOI: 10.1103/PhysRevE.68.026218 PACS number(s): 05.45.Jn, 05.45.Pq, 02.70.Ns, 05.20.Jj

I. INTRODUCTION

Microscopic chaos is one of the essential reasons to justify a statistical treatment of deterministic dynamical systems. In a chaotic system, small initial errors diverge exponentially, as characterized quantitatively by the Lyapunov exponents λ_n, and this means that it is not possible, in principle, to predict precisely all quantities (other than conserved quantities) of deterministic systems and a statistical treatment of the system is required. It is well known that even one-particle systems can be chaotic and have some of the important statistical properties of many-body equilibrium statistical mechanics such as mixing, etc. For this reason, many studies of chaotic behavior have been done in one-particle systems, for example, billiard systems and Lorentz gas models [1,2]. However, many-particle effects should still play an important role in some statistical aspects, such as the central limit theorem, a justification of thermodynamical reservoirs, and critical phenomena, etc. Therefore, it is interesting, in general, to know which aspects of statistical mechanical systems are due to chaos and which are the combination of a chaotic effect and a many-particle effect. In other words, what are the limitations of one-particle systems as models of realistic systems.

The stepwise structure of the Lyapunov spectrum, which was reported numerically in many-hard-disk systems, is one such many-particle chaotic effect [3–5]. Here, the Lyapunov spectrum is introduced as the sorted set $\{\lambda_1,\lambda_2,\ldots\}$ of the Lyapunov exponents satisfying the condition that $\lambda_1 \geqslant \lambda_2 \geqslant \ldots$, and is used to characterize the many-particle chaotic dynamics. The stepwise structure of the Lyapunov spectrum appears in the region of smallest Lyapunov exponents (in absolute value). This fact suggests that steps in the Lyapunov spectra are associated with slow modes and thus the macroscopic behavior of the system. Small positive Lyapunov exponents should correspond to slow growth processes and small negative Lyapunov exponents should correspond to slow relaxation processes. This point is partly supported by the existence of global or cooperative phenomena in the Lyapunov vectors, the so called Lyapunov modes, which are wavelike structures in the eigenvector associated with each degenerate Lyapunov exponent of the stepwise region [4–7]. This wavelike structure of the Lyapunov modes appears as a function of the particle position and possibly the time, so this structure connects the tangent space with the phase space. Although the Lyapunov vectors have been the subject of some studies for more than a decade (for example, see Refs. [8–16]), it is remarkable that an observation of their global structure in fully chaotic hard-core many-particle systems has only recently appeared, despite the observation of stepwise structures in the Lyapunov spectrum of coupled map lattices [8]. A possible reason for this may be the difficulty of observing Lyapunov modes in systems with soft interaction potentials [17]. Explanations for the stepwise structure of the Lyapunov spectra have been attempted using periodic orbit models [18] and using a master equation approach [19]. Other theoretical approaches to the Lyapunov modes have included using a random matrix approach for a one-dimensional model [20], using a kinetic theoretical approach [21], and by considering these as the ''Goldstone modes'' [22].

If the stepwise structure of the Lyapunov spectra is a reflection of a global behavior of the system, then one may ask the question: Does such a structure depend on the boundary conditions or the geometry of the system? One of the purposes of this paper is to answer this question using some simple systems. In this paper, we investigate numerically the stepwise structure of the Lyapunov spectra, and the associated Lyapunov modes, in systems of many hard disks, in two-dimensional rectangular geometry with four different boundary conditions: (P,P), purely periodic boundary conditions; (P,H), periodic boundary conditions in the x direction and hard-wall boundary conditions in the y direction; (H,P), hard-wall boundary conditions in the x direction and periodic boundary conditions in the y direction; and (H,H), purely hard-wall boundary conditions. In all cases, we took

the y direction as the narrow direction of the rectangle and the x direction as the longer orthogonal direction. For case (P,P), the shape of the system is like the surface of a doughnut, for (P,H) and (H,P) the system has the shape of the surface of pipe with hard walls at its ends. Case (H,P) is a long pipe with small diameter while case (P,H) is a short pipe with a large diameter. Case (H,H) is a system of rectangular shape surrounded by hard walls. Adopting hard-wall boundary conditions in a particular direction destroys the spatial translational invariance in that direction, so by considering these models we can investigate the effects of the absence of spatial translational invariance in each direction separately, and in combination, on the stepwise structure of the Lyapunov spectra and existence of the Lyapunov modes. This can be used to check some theoretical approaches to these phenomena such as those in Refs. [19–21], in which the consequences of spatial translational invariance play an essential role in explaining the stepwise structure of the Lyapunov spectra and the Lyapunov modes. We obtain different stepwise structures of the Lyapunov spectra with each different type of boundary condition. In particular, we observe a stepwise structure of the Lyapunov spectrum even in the case of purely hard-wall boundaries (H,H), where the total momentum is not conserved in any direction.

The second purpose of this paper is to categorize the stepwise structure of the Lyapunov spectra according to the wavelike structure of the Lyapunov modes. So far the wavelike structure of the Lyapunov vectors was reported in the Lyapunov vector components as a function of position only, for example, in the quantity $\delta q_{yj}^{(n)}$ as a function of the position q_{xj} (the transverse Lyapunov mode) [4–6] and in the quantity $\delta q_{xj}^{(n)}$ as a function of the position q_{xj} (the longitudinal Lyapunov mode) [7,17], in which $\delta q_{yj}^{(n)}$ ($\delta q_{xj}^{(n)}$) is the y component (x component) of the spatial part of the Lyapunov vector of the jth particle corresponding to the nth Lyapunov exponent λ_n, and q_{xj} is the x component of the spatial component of the jth particle. These wavelike structures appear in the stepwise region of the Lyapunov spectrum. However, it is not clear whether there is a direct connection between the sequence and the kind of steps in the Lyapunov spectrum and the associated Lyapunov modes, that is, how to categorize the steps of the Lyapunov spectrum by their Lyapunov modes. In a two-dimensional system with periodic boundary conditions, the Lyapunov vectors associated with the zero-Lyapunov exponents $(\delta\mathbf{q}_x^{(n)},\delta\mathbf{q}_y^{(n)},\delta\mathbf{p}_x^{(n)},\delta\mathbf{p}_y^{(n)})^T$, $n=2N-2,2N-1,\ldots,2N+3$ can be written as linear combinations of the basis vectors $(\mathbf{a}_0,\mathbf{0},\mathbf{0},\mathbf{0})^T$, $(\mathbf{0},\mathbf{a}_0,\mathbf{0},\mathbf{0})^T$, $(\mathbf{0},\mathbf{0},\mathbf{a}_0,\mathbf{0})^T$, $(\mathbf{0},\mathbf{0},\mathbf{0},\mathbf{a}_0)^T$, $(\mathbf{p}_x,\mathbf{p}_y,\mathbf{0},\mathbf{0})^T$, and $(\mathbf{0},\mathbf{0},\mathbf{p}_x,\mathbf{p}_y)^T$, where T is the transpose, N is the number of particles, $\mathbf{0}$ is an N-dimensional null vector, $\mathbf{a}_0$ is an N-dimensional vector with all components equal, and $\mathbf{p}_x\equiv(p_{x1},p_{x2},\ldots,p_{xN})^T$ [$\mathbf{p}_y\equiv(p_{y1},p_{y2},\ldots,p_{yN})^T$] is the N-dimensional vector whose components are the x component p_{xj} (y component p_{yj}) of the momentum of the jth particle. If we restrict our consideration to the spatial components of the Lyapunov vector, we need only consider basis vectors with nonzero spatial components, that is $(\mathbf{a}_0,\mathbf{0},\mathbf{0},\mathbf{0})^T$, $(\mathbf{0},\mathbf{a}_0,\mathbf{0},\mathbf{0})^T$, and $(\mathbf{p}_x,\mathbf{p}_{yj},\mathbf{0},\mathbf{0})^T$. The Lyapunov vector components $\delta q_{xj}^{(n)}$, $\delta q_{yj}^{(n)}$, $\delta q_{xj}^{(n)}/p_{xj}$, and $\delta q_{yj}^{(n)}/p_{yj}$ correspond to the zero-Lyapunov exponents of the purely periodic system, the first two are associated with spatial translational invariance and the second two with the deterministic nature of the orbit (time translational invariance). In this paper, we show that the quantities $\delta q_{yj}^{(n)}$ and $\delta q_{yj}^{(n)}/p_{yj}$ as a function of q_{xj} are sufficient to categorize the stepwise structure of the Lyapunov spectra of a quasi-one-dimensional system. More concretely, we consider two types of Lyapunov modes: the quantity $\delta q_{yj}^{(n)}$ as a function of the position q_{xj}, the transverse (spatial translational invariance) Lyapunov mode $[Ts]$, and the quantity $\delta q_{yj}^{(n)}/p_{yj}$ as a function of the position q_{xj} and time (or collision number), the transverse time translational invariance Lyapunov mode $[Tt]$. In two-dimensional rectangular systems consisting of many hard disks with periodic boundary conditions (P,P), it is known that there are two types of steps of the Lyapunov spectra: steps of degeneracy two and steps of degeneracy four [5,6]. The Lyapunov vectors associated with the two-point steps of the Lyapunov spectrum are known to contain a wavelike structure of type $[Ts]$ for a rectangular system. In this paper, we show that the wavelike structure corresponding to the four-point steps of the Lyapunov spectrum is of type $[Tt]$. Further, we observe time-dependent oscillations in the mode $[Tt]$, whereas the mode $[Ts]$ is stationary in time. The wavelike structure of type $[Tt]$ also appears in rectangular systems with hard-wall boundary conditions [that is, for (P,H), (H,P), and (H,H)], and specifically in the case of purely hard-wall boundary conditions where the transverse Lyapunov mode $[Ts]$ does not appear. We show that the stepwise structure of the Lyapunov spectra in the boundary cases (P,P), (P,H), (H,P), and (H,H) can be completely categorized by wavelike structures of types $[Ts]$ and $[Tt]$.

One of the problems that make it difficult to investigate the structure of the Lyapunov spectra and the Lyapunov modes is that the calculation of a full Lyapunov spectra for a many-particle system is a very time-consuming numerical calculation. Therefore, it is important to use a system in which the stepwise structure of the Lyapunov spectra and the Lyapunov modes can be calculated as quickly as possible. It is known that a rectangular system has a wider stepwise region in the Lyapunov spectrum than a square system (of the same area) [5]. Noting this, in this paper we concentrate on the most strongly rectangular system, namely a quasi-one-dimensional system, in which the rectangle is so narrow that particles cannot exchange their positions, thus the order of the particles is maintained and collisions can only occur between neighboring particles. As will be shown in this paper, the stepwise structure of the Lyapunov spectrum for the quasi-one-dimensional system is the same as for the fully rectangular system which allows exchange of particle positions and collisions between any pair of particles, and the steps of the Lyapunov spectra consist of two-point steps and four-point steps, for the fully periodic case (P,P). Another advantage of using the quasi-one-dimensional system is that in this system the roles of the x direction and y direction are separate, so, for example, we can expect the most clear difference when applying hard-wall boundary in each case,

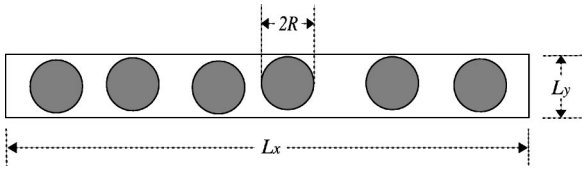

FIG. 1. Quasi-one-dimensional system: A narrow rectangular system satisfying the conditions $RN\sqrt{3}<L_x$ and $2R<L_y<4R$.

(P,H) and (H,P). We also investigate the particle density dependence of the Lyapunov spectrum to find a state in which the two-point steps are most clearly distinguished from the four-point steps.

The outline of this paper is as follows. In Sec. II, we discuss in detail the quasi-one-dimensional system and the dependence of the Lyapunov spectrum on the number of hard disks N and the density. In Sec. III, we consider the purely periodic boundary condition case (P,P), and investigate wavelike structures of types $[Ts]$ and $[Tt]$ in the Lyapunov vectors. In Sec. IV, we consider other boundary conditions, in particular, hard-wall boundary conditions in the y direction (P,H), and in the x direction (H,P), and then purely hard-wall boundaries (H,H), and investigate the existence of modes of types $[Ts]$ and $[Tt]$ in their Lyapunov vectors. Results for the four different boundary conditions are compared. Finally, we give some conclusions and remarks in Sec. V.

II. QUASI-ONE-DIMENSIONAL SYSTEMS AND DENSITY DEPENDENCE OF THE LYAPUNOV SPECTRUM

The stepwise structure of the Lyapunov spectra is purely a many-particle effect of the chaotic dynamics, and so far it has been investigated in systems of 100 or more particles. However, the numerical calculation of the Lyapunov spectra for such large systems is very time consuming. Noting this point, in this section we discuss how we can investigate the stepwise structure of the Lyapunov spectrum for a system whose number of particles is as small as possible. We also investigate the particle density dependence of the Lyapunov spectrum in order to choose system parameters which give the clearest differentiation of the stepwise structure.

We consider two-dimensional systems consisting of N hard disks in which the radius of the particle is R and the width (height) of the system is L_x (L_y). One way to get the stepwise structure of the Lyapunov spectrum in a two-dimensional system consisting of a small number of particles is to choose a rectangular system rather than a square system (of the same N and area), because the stepwise region in the Lyapunov spectrum is wider in a more rectangular system [5]. Noting this characteristic, we concentrate on the most rectangular case, namely, the quasi-one-dimensional system defined by the conditions

$$RN\sqrt{3}<L_x \quad \text{and} \quad 2R<L_y<4R. \tag{1}$$

A schematic illustration of the quasi-one-dimensional system is shown in Fig. 1. This quasi-one-dimensional system is a narrow rectangular system where each particle can only interact with two nearest-neighbor particles, and particles remain in the same order. In the quasi-one-dimensional system, the upper bound ρ_{max} on the particle density $\rho \equiv N\pi R^2/(L_xL_y)$ [23] is given by $\rho_{max}=\pi/(2\sqrt{3}) = 0.9068\ldots$ in the purely periodic boundary conditions and $\rho_{max}=\pi/4=0.7853\ldots$ in the purely hard-wall boundary conditions. In such a system, we get a stepwise structure in the Lyapunov spectrum even in a system as small as $N=10$, as shown in Fig. 2, where the Lyapunov spectrum is normalized by the maximum Lyapunov exponent $\lambda_1\approx 3.51$. To get this figure, we chose the parameters as $R=1$, $L_y=2R(1+10^{-6})$, $L_x=NL_y(1+10^{-3})$, and the mass M of the particle and the total energy E are given by 1 and N, respectively, and we used purely periodic boundary conditions. The particle density of this system is given by $\rho=0.7846\ldots$. Noting the pairing property of the Lyapunov spectrum for Hamiltonian systems, namely, the property that in Hamiltonian systems any positive Lyapunov exponent accompanies a negative Lyapunov exponent with the same absolute value [1,24], we plotted the first half of the Lyapunov spectrum in Fig. 2. (The negative branch of the Lyapunov spectra will be omitted from all subsequent plots.) It is clear that the Lyapunov exponents λ_{16} and λ_{17} form a two-point step in this spectrum.

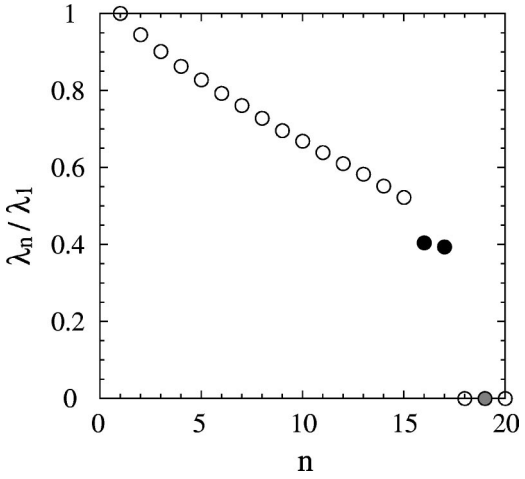

FIG. 2. The Lyapunov spectrum normalized by the maximum Lyapunov exponent for a ten-hard-disk system with the periodic boundary conditions in both directions. The Lyapunov exponents λ_{16} and λ_{17} shown as the black circles form a two-point step associated with the transverse Lyapunov modes shown in Fig. 3. The gray circle is the zero-Lyapunov exponent λ_{19} whose corresponding Lyapunov vector components $\delta q_{yj}^{(n)}$ show a constant behavior (also see Fig. 3).

In order to calculate the Lyapunov spectra and the Lyapunov vectors we use the algorithm due to Benettin *et al.*, which is characterized by intermittent rescaling and renormalization of Lyapunov vectors [25,26]. In the application of this algorithm to systems with hard-core particle interactions, we calculate the matrix $\Lambda(t_k)$, whose column vectors give the Lyapunov vectors $\delta\mathbf{\Gamma}_n(t_k)$ corresponding to the local-time Lyapunov exponent $\tilde{\lambda}_n(t_k)$ at time $t=t_k$ just after the kth collision in the system. The dynamics of the matrix $\Lambda(t_k)$ is given by $\Lambda(t_{k+1})=\mathcal{N}_k\mathcal{G}_k\mathcal{M}_k\Lambda(t_k)$, in which

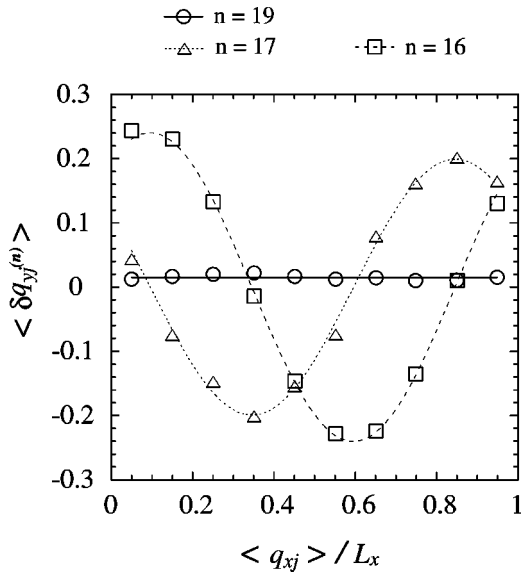

FIG. 3. The time-averaged y components $\langle \delta q_{yj}^{(n)} \rangle$ of the Lyapunov vector of the jth particle as functions of the time average $\langle q_{xj} \rangle / L_x$ of the normalized x component of the position of the jth particle corresponding to the Lyapunov exponents λ_{19}, λ_{17}, and λ_{16}, in the ten-hard-disk system with the periodic boundary conditions in both directions. The circle, triangle, and square dots correspond to the Lyapunov exponents λ_{19}, λ_{17}, and λ_{16}, respectively, which are shown as the gray-and black-filled circles in Fig. 2. The dotted and dashed lines are the fitting lines for the sinusoidal functions, and the solid line is the fit for the constant function.

$\mathcal{N}_k$ is the matrix required to normalize each column vector in the operated matrix $\mathcal{G}_k \mathcal{M}_k \Lambda(t_k)$, $\mathcal{G}_k$ is the Gram-Schmidt procedure ensuring the orthogonality of the columns in the operated matrix, and $\mathcal{M}_k$ specifies the tangent space dynamics including a free flight and a particle collision [3]. The local-time Lyapunov exponent $\tilde{\lambda}_n(t_k)$ is calculated as the rate of the exponential divergence (contraction) of the nth column vector of the matrix $\Lambda(t_k)$ to the nth column vector of the matrix $\mathcal{G}_k \mathcal{M}_k \Lambda(t_k)$. The Lyapunov exponent λ_n is given as a time-averaged local-time Lyapunov exponent after a long time calculation: $\lambda_n = \lim_{k\to\infty} \tilde{\lambda}_n(t_k)$. Here we use the standard metric $d\delta s^2 = \Sigma_{j=1}^{N} (d\delta q_{xj}^{(n)2} + d\delta q_{yj}^{(n)2} + d\delta p_{xj}^{(n)2} + d\delta p_{yj}^{(n)2})$ for the tangent space with the x component $\delta p_{xj}^{(n)}$ and y component $\delta p_{yj}^{(n)}$ of the Lyapunov vector of the jth particle corresponding to the local-time Lyapunov exponent $\tilde{\lambda}_n$. Other papers such as Refs. [3,27,28] should be referred to for more details of the Benettin algorithm and the tangent space dynamics of many-hard-disk systems.

It is very important to note that there are two ways that convince us of the structure of the Lyapunov spectrum; one is simply to find a step structure directly in the Lyapunov spectrum, and another is to find a structure in the Lyapunov vectors corresponding to a specific Lyapunov exponent. Figure 3 is the plot of the time average $\langle \delta q_{yj}^{(n)} \rangle$ of the y component of the jth particle contribution to the Lyapunov vector $\delta \mathbf{\Gamma}_n$ corresponding to the Lyapunov exponents λ_{19}, λ_{17}, and λ_{16} as functions of the time average $\langle q_{xj} \rangle / L_x$ of the normalized x component of the jth particle (for $j = 1,2,\ldots,N$) (the graph $[Ts]$). The corresponding Lyapunov exponents λ_{17} and λ_{16} are shown as the black-filled circles in Fig. 2 and form a two-point step in the Lyapunov spectrum. The time average of the quantities $\delta q_{yj}^{(n)}$ and q_{xj} is the arithmetic average of the quantity immediately after collision, taken over $100N$ collisions. The step consisting of two points in the Lyapunov spectrum of Fig. 2 accompanies wavelike structures in their Lyapunov vectors, which are called the transverse spatial translational invariance Lyapunov modes. It should be emphasized that the Lyapunov modes in Fig. 3 are stationary over $100N$ collisions and the time average sharpens their wavelike structures. In this figure, we fitted the numerical data for the Lyapunov modes corresponding to the Lyapunov exponents λ_{17} and λ_{16}, to obtain the functions $y = \alpha_n \cos(2\pi x + \beta_n)$ $[(\alpha_{17}, \beta_{17}) = (0.199\,13, 0.9703)$ for the triangle dots, and $(\alpha_{16}, \beta_{16}) = (0.240\,25, -0.596\,77)$ for the square dots]. It should be noted that the difference $\beta_{17} - \beta_{16} = 0.9703 - (-0.596\,77) = 1.567\,07$ of the two values of the phases β_n is approximately $\pi/2 = 1.570\ldots$, meaning that these two waves are orthogonal to each other. As the Benettin algorithm returns orthonormal Lyapunov vectors, α_n in the fits are simply normalization constants. The graph of the Lyapunov vector component $\delta q_{yj}^{(n)}$ as a function of the position q_{xj} $(j = 1,2,\ldots,N)$ becomes constant in one of the zero-Lyapunov exponent λ_{19} shown as the gray-filled circle in Fig. 2. In Fig. 3, we also fitted the numerical data corresponding to the zero-Lyapunov exponent λ_{19} by the constant function $y = \alpha_{19}$ with the fitting parameter value $\alpha_{19} = 0.015\,114$.

Although we can recognize the two-point step of the Lyapunov spectrum in Fig. 2, it is important to note that there is another type of step in the two-dimensional hard-disk system with a rectangular shape and periodic boundary conditions. It is well known that in larger systems the Lyapunov spectrum can have a stepwise structure consisting of both two-point and four-point steps [5,21]. If we want to investigate the four-point steps, we have to consider a system consisting of more than ten particles.

Another interesting property of the Lyapunov vectors is the angle θ_n between their coordinate space direction $\delta \mathbf{q}^{(n)}$ and their momentum space direction $\delta \mathbf{p}^{(n)}$, $\delta \mathbf{\Gamma}_n = (\delta \mathbf{q}^{(n)}, \delta \mathbf{p}^{(n)})^T$, where θ_n is defined by [21]

$$\theta_n \equiv \cos^{-1}\left(\frac{\delta \mathbf{q}^{(n)} \cdot \delta \mathbf{p}^{(n)}}{|\delta \mathbf{q}^{(n)}||\delta \mathbf{p}^{(n)}|} \right). \tag{2}$$

Figure 4 is the graph for the time average $\langle \theta_n \rangle$ as a function of exponent number n except for the ones corresponding to the zero-Lyapunov exponents. Here, again the time average of the angle θ_n is the arithmetic average of the values immediately after collisions, for $1000N$ collisions.

In Fig. 4, we also plotted the angles θ_n at an instant time in order to know magnitudes of their fluctuations. This graph shows that the spatial part $\delta \mathbf{q}^{(n)}$ and the momentum part $\delta \mathbf{p}^{(n)}$ of the Lyapunov vector are pointed in almost the same direction for $n = 1,2,\ldots,2N-3$ and in almost the opposite direction for $n = 2N+4, 2N+5, \ldots, 4N$. This fact suggests that if we get a structure in the vector $\delta \mathbf{q}^{(n)}$, then we may

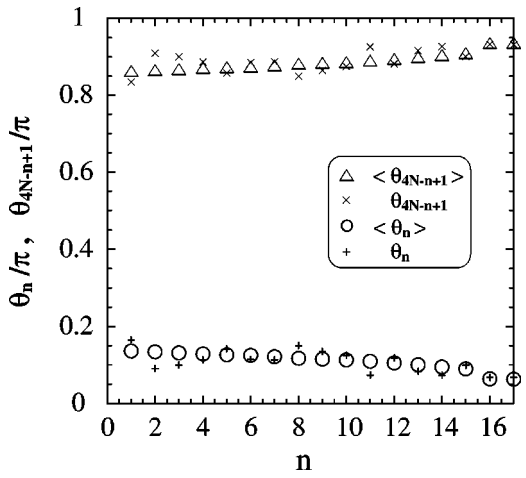

FIG. 4. Time-averaged angle $\langle \theta_n \rangle$ and instantaneous angles θ_n between the spatial part $\delta\mathbf{q}^{(n)}$ and the momentum part $\delta\mathbf{p}^{(n)}$ of the Lyapunov vector $\delta\mathbf{\Gamma}_n=(\delta\mathbf{q}^{(n)},\delta\mathbf{p}^{(n)})^T$ corresponding to the Lyapunov exponent λ_n in the ten-hard-disk system with the periodic boundary conditions in both directions.

expect a similar structure in the vector $\delta\mathbf{p}^{(n)}$, and vice versa. It should also be noted that this gives a justification for some approaches to the Lyapunov exponents in which the Lyapunov exponents are calculated through the spatial coordinate part only (or the momentum part) of the Lyapunov vector [18,29]. For this reason, in this paper we concentrate mainly on the structure of the spatial part of the Lyapunov vectors, and omit discussion of the structure of the momentum part. Using the symplectic property of Hamiltonian dynamics, if the Lyapunov vector $\delta\mathbf{\Gamma}_n=(\delta\mathbf{q}^{(n)},\delta\mathbf{p}^{(n)})^T$ corresponds to the Lyapunov exponent λ_n, then its conjugate Lyapunov vector $\delta\mathbf{\Gamma}_{4N-n+1}=(\delta\mathbf{q}^{(4N-n+1)},\delta\mathbf{p}^{(4N-n+1)})^T$ corresponding to the Lyapunov exponent $\lambda_{4N-n+1}=-\lambda_n$ is $\delta\mathbf{\Gamma}_{4N-n+1}=\pm(\delta\mathbf{p}^{(n)},-\delta\mathbf{q}^{(n)})^T$ [1], so the graph of θ_n, $n=1,2,\ldots,2N-3$, and θ_{4N-n+1}, $n=1,2,\ldots,2N-3$, is symmetric with respect to the line $\theta_n/\pi=1/2$ at any instant of time, because $\delta\mathbf{q}^{(4N-n+1)}\cdot\delta\mathbf{p}^{(4N-n+1)}=-\delta\mathbf{q}^{(n)}\cdot\delta\mathbf{p}^{(n)}$.

Another important point to obtain a clear stepwise structure in the Lyapunov spectrum is the choice of the particle density. Even if we restrict our consideration to quasi-one-dimensional systems, the shape of the Lyapunov spectrum depends on the particle density, so we should choose a density that gives a clearly visible stepwise structure in the Lyapunov spectrum with two-point steps differentiated from four-point steps. Figure 5(a) is the Lyapunov spectra normalized by the maximum Lyapunov exponent for a quasi-one-dimensional system of 50 hard disks ($N=50$) with periodic boundary conditions in both directions. We also give an enlarged Fig. 5(b) for the small Lyapunov exponent region. Here the system parameters are given by $R=1$, $L_y=2R(1+10^{-6})$, $L_x=NL_y(1+d)$, and we used $M=1$ and $E=N$. The five Lyapunov spectra correspond to the states of $d=10^{-4}$ (circles, $\rho=0.7853\ldots$), $d=10^{-1}$ (triangles, $\rho=0.7139\ldots$), $d=1$ (squares, $\rho=0.3926\ldots$), $d=10$ (diamonds, $\rho=0.07\,139\ldots$), $d=10^2$ (inverted triangles, $\rho=0.007\,776\ldots$). The maximum Lyapunov exponents λ_1 are given approximately by 3.62, 2.44, 0.934, 0.279, and 0.0579, respectively. As shown in Figs. 5(a) and 5(b), for smaller values of the quantity d (that is, higher particle density), the gaps between the nearest steps of the Lyapunov spectrum become larger, although the stepwise region of the Lyapunov spectrum does not seem to depend on the quantity d. This means that we can get a clear stepwise structure for the Lyapunov spectrum in the small d case (that is, at high density).

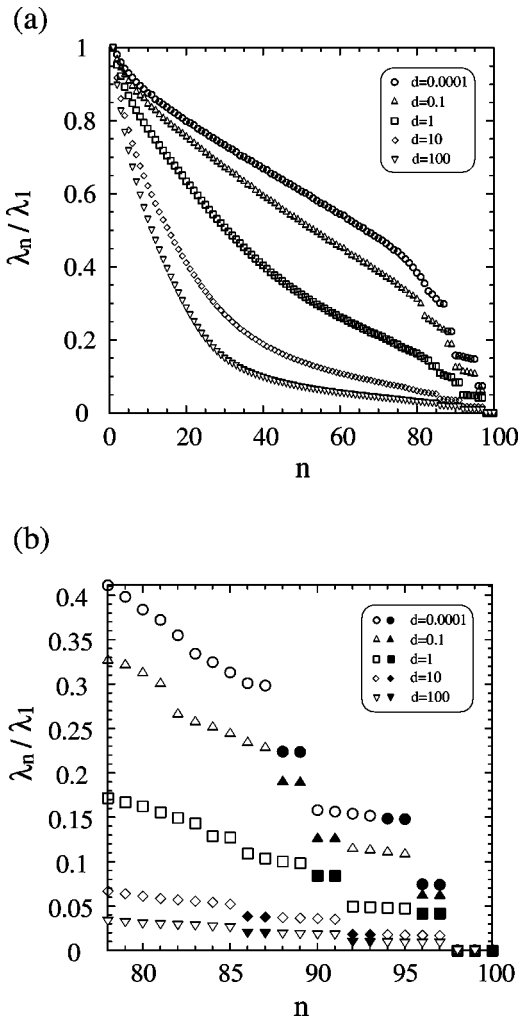

FIG. 5. The density dependence of the Lyapunov spectrum normalized by the maximum Lyapunov exponent for the quasi-one-dimensional system with $N=50$ and periodic boundary conditions in both directions. The five Lyapunov spectra correspond to $L_y=2R(1+10^{-6})$, $L_x=NL_y(1+d)$ with $d=10^{-4}$ (circles), $d=10^{-1}$ (triangles), $d=1$ (squares), $d=10$ (diamonds), $d=10^2$ (inverted triangles). (a) Full scale. (b) The small positive Lyapunov exponent region including the stepwise structure of the Lyapunov spectra. In (b), filled black symbols correspond to the Lyapunov exponents for which the time-averaged Lyapunov vector components $\langle \delta q_{yj}^{(n)} \rangle$ as a function of $\langle q_{xj} \rangle$ show wavelike structures. Filled gray symbols are for the Lyapunov vectors whose behavior is constant.

In Fig. 5(b), the Lyapunov exponents accompanying wavelike structures (constant behaviors) in the time-averaged Lyapunov vector components $\langle \delta q_{yj}^{(n)} \rangle$, as functions of the position $\langle q_{xj} \rangle$, are shown as the black (gray) symbols. In the

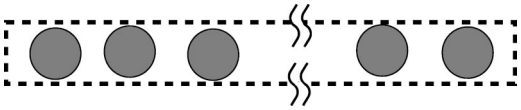

FIG. 6. A schematic illustration of a quasi-one-dimensional system with periodic boundary conditions in both directions. The dashed lines indicate periodic boundary conditions along that boundary.

small d case, looking from the zero-Lyapunov exponents, the two-point step appears first [see $d=10^{-4}$, 10^{-1} and 1 in Fig. 5(b)], whereas the four-point step appears first in the large d case (see $d=10^{1}$ and $d=10^{2}$). Besides, at least in the small d case, the two-point steps and four-point steps do not appear repeatedly (see $d=10^{-4}$ and 10^{-1}). These facts mean that the sequence of steps in the Lyapunov spectrum depends on the quantity d, and therefore on the particle density.

The wavelike structures in the time-averaged Lyapunov vector components $\langle \delta q_{yj}^{(n)} \rangle$ as functions of the position $\langle q_{xj} \rangle$ (namely, the transverse spatial translational invariance Lyapunov modes) appear mainly in the two-point steps of the Lyapunov spectra. Therefore, we can use these wavelike structures to distinguish two-point steps from four-point steps in the Lyapunov spectra. However, such a criterion sometimes seems to fail in steps of the Lyapunov spectra near a region where the spectra are changing smoothly. Actually, the transverse Lyapunov modes may appear even in some apparently four-point steps, if they are near such a smoothly changing Lyapunov spectrum region. On the other hand, in such a region of the Lyapunov spectra, the fluctuations of Lyapunov vectors are rather large, and the wavelike structure becomes vague. In Fig. 5(b), we did not indicate with black-filled symbols the Lyapunov exponents whose corresponding Lyapunov vector components $\langle \delta q_{yj}^{(n)} \rangle$ as functions of the position $\langle q_{xj} \rangle$ show vague wavelike structures.

Based on the discussions in this section, in the following two sections we consider only the case with system parameters given by $N=75$, $R=1$, $M=1$, and $E=N$. The height and the width of the system are given by $L_y=2R(1+10^{-6})$ and $L_x=1.5NL_y$ (the density $\rho=0.5235\ldots$) for the purely periodic boundary case. In this case, as will be shown in the following section, we can recognize at least two clear sequences of two-point steps then four-point steps, in the Lyapunov spectrum for this system. We always take the time-averaged quantities $\langle \delta q_{yj}^{(n)} \rangle$ and $\langle q_{xj} \rangle$ of the quantities $\delta q_{yj}^{(n)}$ and q_{xj}, respectively, as the arithmetic average of their values taken at times immediately after collisions, over $100N$ collisions. We calculated more than 2×10^{5} collisions (10^{6} collisions in some of the models) in order to get the Lyapunov spectra and the Lyapunov vectors in the models presented in this paper.

III. QUASI-ONE-DIMENSIONAL SYSTEMS WITH PERIODIC BOUNDARY CONDITIONS

In this section, we consider the Lyapunov spectrum for the quasi-one-dimensional system with periodic boundary conditions in both the directions (P,P). A schematic illustration of this system for latter comparisons is given in Fig. 6

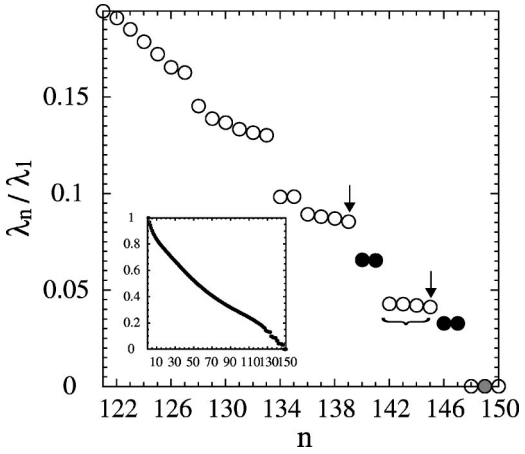

FIG. 7. The stepwise structure of the Lyapunov spectrum normalized by the maximum Lyapunov exponent for a quasi-one-dimensional system with periodic boundary conditions in both directions. Inset: Full scale for the normalized Lyapunov spectrum. The circles are filled black (gray) in the Lyapunov exponents corresponding to wavelike structures (constant behavior) of the time-averaged Lyapunov vector components $\langle \delta q_{yj}^{(n)} \rangle$ shown in Fig. 8.

in which the dashed line along the boundary means periodic boundary conditions. This system satisfies spatial translational invariance in both directions, and is regarded as a reference model for the models considered in the following section.

Figure 7 is the small positive Lyapunov exponent region of the Lyapunov spectrum normalized by the maximum Lyapunov exponent $\lambda_1\approx1.33$, including its stepwise region, for a quasi-one-dimensional system with periodic boundary conditions in both the directions. The global shape of the Lyapunov spectrum is given in the inset in this figure. We used the values of the system parameters chosen at the end of the preceding section. At least five steps consisting of three two-point steps and two four-point steps are clearly visible in this Lyapunov spectrum with the sequence of steps being 2-4-2-4-2.

The two-point steps of the Lyapunov spectrum accompany wavelike structures in their corresponding Lyapunov vectors. Figure 8 is the graph of the time-averaged Lyapunov vector components $\langle \delta q_{yj}^{(n)} \rangle$ corresponding to the Lyapunov exponents λ_{149}, λ_{147}, λ_{146}, λ_{141} and λ_{140}, as functions of the time-averaged position component $\langle q_{xj} \rangle$ normalized by the length L_x (the mode $[Ts]$). The Lyapunov exponents used for this figure are shown as the black or gray circles in Fig. 7. In this figure, we also give fits of the numerical data to sinusoidal equations or a constant function (where appropriate). The fitting equations are $y=\alpha_n\cos(2\pi x+\beta_n)$ for $n=147,146$ $[(\alpha_{147},\beta_{147})=(-0.16\,132,-4.5575)$, $(\alpha_{146},\beta_{146})=(-0.161\,25,0.149\,28)]$, and $y=\alpha_n\cos(4\pi x+\beta_n)$ for $n=141,140$ $[(\alpha_{141},\beta_{141})=(-0.157\,75,-0.305\,81)$, $(\alpha_{140},\beta_{140})=(0.157\,82,1.2666)]$. It is important to note the relations $|\alpha_{147}|\approx|\alpha_{146}|$, $|\alpha_{141}|\approx|\alpha_{140}|$, $\beta_{146}-\beta_{147}\approx3\pi/2$, and $\beta_{140}-\beta_{141}\approx\pi/2$, meaning that the two wavelike structures in the same two-point step are orthogonal to each other. In Fig. 8, we also draw a graph of the averaged Lyapunov vector component $\langle \delta q_{yj}^{(n)} \rangle$ as a function

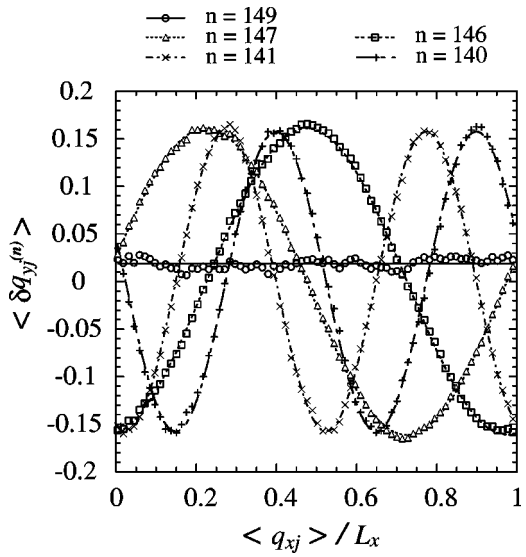

FIG. 8. The time-averaged Lyapunov vector components $\langle \delta q_{yj}^{(n)} \rangle$ as functions of the time average $\langle q_{xj} \rangle / L_x$ of the normalized x component of the jth particle for the Lyapunov exponents λ_{149}, λ_{147}, λ_{146}, λ_{141}, and λ_{140} for the quasi-one-dimensional system with the periodic boundary conditions in both directions. The corresponding Lyapunov exponents are shown as the gray- and black-filled circles in Fig. 7. The numerical data are fitted by a constant function and sinusoidal functions.

of the normalized position $\langle q_{xj} \rangle / L_x$ corresponding to the second zero-Lyapunov exponent λ_{149}, which is approximately constant, and is fitted by a constant function $y = \alpha_{149}$ with the fitting parameter value $\alpha_{149} = 0.018\,901$. These results suggest the following conjecture for the approximate form of the Lyapunov vector components $\delta q_{yj}^{[n(k)]}$ and $\delta q_{yj}^{[n(k)-1]}$ corresponding to the Lyapunov exponents $\lambda_{n(k)}$ and $\lambda_{n(k)-1}$ in the same kth two-point step counting from the zero-Lyapunov exponents as

$$\{\delta q_{yj}^{[n(k)]}, \delta q_{yj}^{[n(k)-1]}\} \approx \left\{ \alpha_k \cos\left(\frac{2\pi k}{L_x} q_{xj} + \beta_k \right), \alpha_k \sin\left(\frac{2\pi k}{L_x} q_{xj} + \beta_k \right) \right\}, \tag{3}$$

$j = 1,2,\ldots,N$ with constants α_k and β_k. (Note that we count the sequence of steps of the Lyapunov spectra beginning from the zero-Lyapunov exponents, so for example, the first two-point step consists of exponents λ_{147} and λ_{146} and the second two-point step consists of exponents λ_{141} and λ_{140} in Fig. 7.) Note that the constant α_k in Eq. (3) is determined by the normalization condition for the Lyapunov vector in Benettin's algorithm.

It should be emphasized that the wavelike structures in Figs. 3 and 8 correspond to the two-point steps of the Lyapunov spectrum. We cannot recognize such a clear wavelike structure in the graph of the Lyapunov vector component $\langle \delta q_{yj}^{(n)} \rangle$ as a function of the position $\langle q_{xj} \rangle$ for the four-point steps in the Lyapunov spectrum. This suggests that the physical meaning of the four-point steps is different from that of two-point steps, and we should consider a different quantity to characterize the Lyapunov vectors of the four-point steps. Now, as one of the important results of this paper, we show that the wavelike structures in the quantities $\delta q_{yj}^{(n)} / p_{yj}$ as functions of q_{xj} and the collision number appear in the four-point steps of the Lyapunov spectrum. As a motivation for the introduction of the quantity $\delta q_{yj}^{(n)} / p_{yj}$, we note that a small perturbation of the spatial coordinates of the particles in the direction of the orbit, namely, $\delta \mathbf{q} \propto \mathbf{p}$, leads to a zero-Lyapunov exponent, so that the quantities $\delta q_{yj}^{(n)} / p_{yj}$, $j = 1,2,\ldots,N$, should give a constant value corresponding to this zero-Lyapunov exponent. This is the common feature as the quantity $\delta q_{yj}^{(n)}$, which shows a constant behavior corresponding to one of the zero-Lyapunov exponents due to spatial translational invariance, and whose wavelike structure we have already discussed.

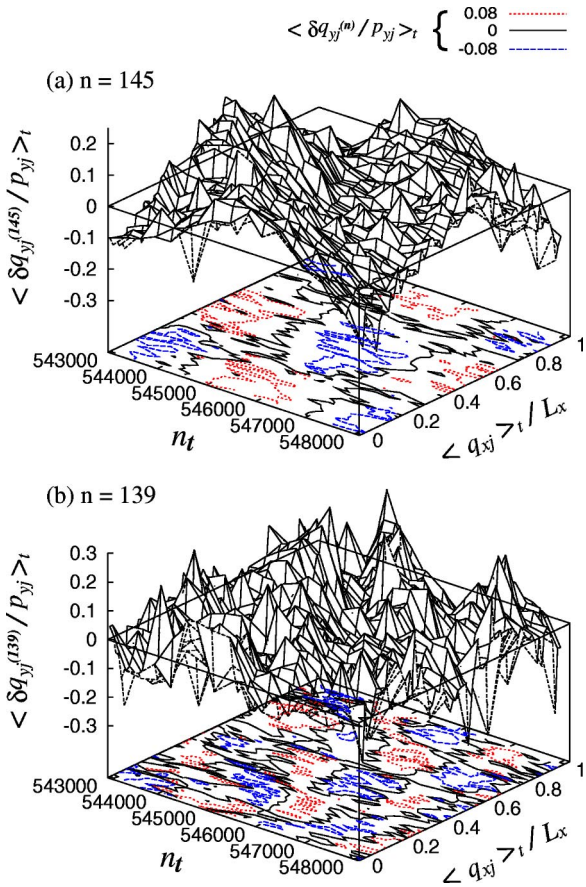

FIG. 9. Local time-averaged quantities $\langle \delta q_{yj}^{(n)} / p_{yj} \rangle_t$ as functions of the normalized position $\langle q_{xj} \rangle_t / L_x$ and the collision number n_t corresponding to (a) the Lyapunov exponent λ_{142} in the first four-point step and (b) the Lyapunov exponent λ_{139} in the second four-point step in the same collision number interval [543 000,548 100]. The system is the quasi-one-dimensional system with the periodic boundary conditions in both directions, and the corresponding Lyapunov exponents are indicated by arrows in Fig. 7. In the contour plots on the bottoms of these three-dimensional plots, dotted lines, solid lines, and dashed lines correspond to the values $\langle \delta q_{yj}^{(n)} / p_{yj} \rangle_t = 0.08$, 0, and -0.08, respectively.

For the introduction of the quantity $\delta q_{yj}^{(n)} / p_{yj}$, we note that a small perturbation of the spatial coordinates of the particles in the direction of the orbit, namely, $\delta \mathbf{q} \propto \mathbf{p}$, leads to a zero-Lyapunov exponent, so that the quantities $\delta q_{yj}^{(n)} / p_{yj}$, $j = 1,2,\ldots,N$, should give a constant value corresponding to this zero-Lyapunov exponent. This is the common feature as the quantity $\delta q_{yj}^{(n)}$, which shows a constant behavior corresponding to one of the zero-Lyapunov exponents due to spatial translational invariance, and whose wavelike structure we have already discussed.

Before showing graphs of $\delta q_{yj}^{(n)} / p_{yj}$, we discuss some

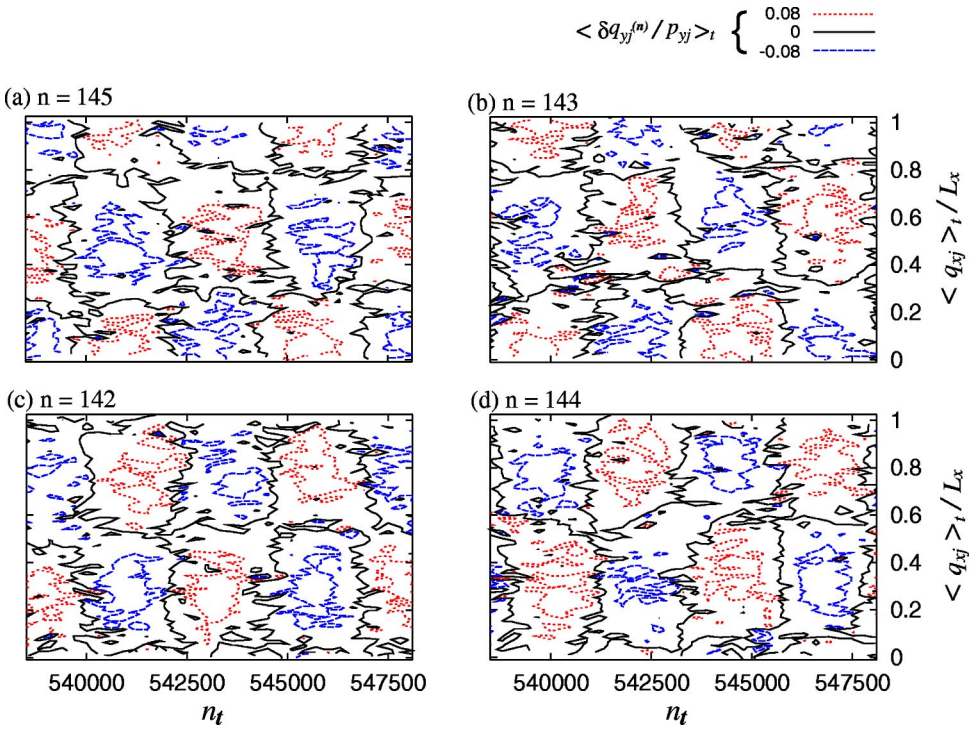

FIG. 10. Contour plots of the local-time averaged quantities $\langle \delta q_{yj}^{(n)}/p_{yj}\rangle_t$ as functions of the normalized position $\langle q_{xj}\rangle_t/L_x$ and the collision number n_t corresponding to the first four-point step consisting of the Lyapunov exponents λ_{145}, λ_{144}, λ_{143}, and λ_{142}, in the same collision number interval [538 500,548 100]. Here dotted lines, solid lines, and dashed lines correspond to the values $\langle \delta q_{yj}^{(n)}/p_{yj}\rangle_t = 0.08$, 0, and -0.08, respectively. The system is the quasi-one-dimensional system with periodic boundary conditions in both directions, and the corresponding Lyapunov exponents are those indicated by the brace under open circles in Fig. 7.

difficulties in the investigation of wavelike structure in these quantities. It is much harder to observe the wavelike structure in these quantities corresponding to the four-point steps, compared to the quantities $\delta q_{yj}^{(n)}$ corresponding to the two-point steps, for at least two reasons. First, the fluctuations in the wavelike structure of the quantities $\delta q_{yj}^{(n)}/p_{yj}$ is much larger than those in the wavelike structure of the quantities $\delta q_{yj}^{(n)}$, partly because the fluctuation is magnified when p_{yj} appearing in the denominator has a small absolute value. Second, the wavelike structure of the quantity $\delta q_{yj}^{(n)}/p_{yj}$ oscillates periodically in time, whereas the wavelike structure of the quantities $\delta q_{yj}^{(n)}$ in Fig. 8 is stationary at least over more than $100N$ collisions. This fact gives an upper bound on the time period (or the collision number interval) over which we can take the time average of $\delta q_{yj}^{(n)}/p_{yj}$ in order to suppress the fluctuations and still get their clear wavelike structures. In this paper, we express the local time averages of the quantities $\delta q_{y}^{(n)}/p_{yj}$ and q_{xj} as $\langle \delta q_{yj}^{(n)}/p_{yj}\rangle_t$ and $\langle q_{xj}\rangle_t$, respectively, with the suffix t to remind us that they can change in time.

In this and the following, sections, we will give the graphs of $\delta q_{yj}^{(n)}/p_{yj}$ as functions of q_{xj} and the collision number by taking their local time averages, so here we summarize how we calculate the data for those graphs from a technical point of view. First we take the arithmetic time average $\langle \delta q_{yj}^{(n)}/p_{yj}\rangle_t$ and $\langle q_{xj}\rangle_t$ of the quantities $\delta q_{yj}^{(n)}/p_{yj}$ and q_{xj}, respectively, using their values just after particle collisions over $4N$ collisions ($8N$ collisions), but if the absolute value $|p_{yj}|$ of the momentum is less than 5% (10%) of the averaged momentum amplitudes $\sqrt{2ME/N}$, then we exclude the quantity $\delta q_{yj}^{(n)}/p_{yj}$ at that time from samples to take this local time average, in the models of this section and Sec. IV A (in the models of the Secs. IV B and IV C). [Therefore, the sample number for taking the arithmetic averages can be less than $4N$ ($8N$) in the models of this section and Sec. IV A (in the models of Secs. IV B and IV C).] Even with this local time average, we can still get more than ten locally time-averaged data points per period for the modes with the slowest time-oscillating movement of the quantity $\delta q_{yj}^{(n)}/p_{yj}$ corresponding to a step of the Lyapunov spectra, for example, corresponding to the first four-point step of the model in this section. In this paper, we consider the graph of the quantity $\langle \delta q_{yj}^{(n)}/p_{yj}\rangle_t$ as a function of $\langle q_{xj}\rangle_t$ and n_t, where n_t is the first collision number contained in the interval over which the time average is taken, $\langle\cdots\rangle_t$.

Figures 9(a) and 9(b) are the graphs of the quantity $\langle \delta q_{yj}^{(n)}/p_{yj}\rangle_t$ as functions of the normalized position $\langle q_{xj}\rangle_t/L_x$ and the collision number n_t, corresponding to the Lyapunov exponents λ_{145} and λ_{139}, respectively, indicated by arrows in Fig. 7. These two graphs correspond to the Lyapunov exponents in different four-point steps and the same collision number interval is used, [543 000,548 100]. In the graph corresponding to the Lyapunov exponent λ_{145} (λ_{139}), we can recognize a spatial wavelike structure of wavelength 1 (1/2) oscillating in time. The time-oscillating period corresponding to the Lyapunov exponent λ_{139} is about

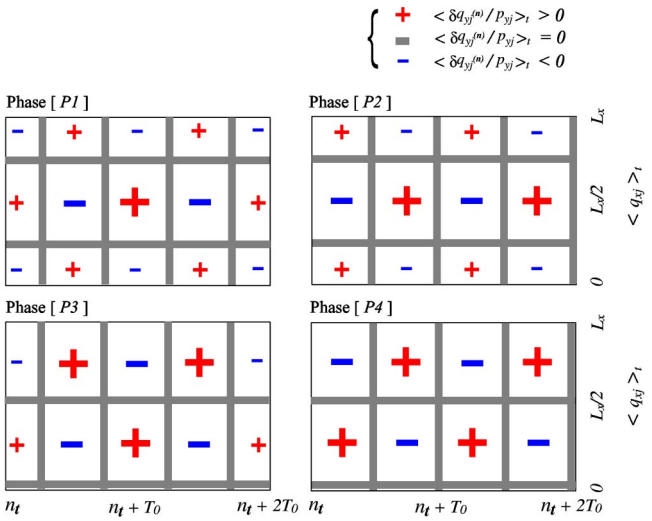

FIG. 11. A schematic illustration of the phase relations amongst the four time-oscillating wavelike structures for the quantities $\langle \delta q_{yj}^{(n)}/p_{yj}\rangle_t$ as functions of the position $\langle q_{xj}\rangle_t$ and the collision number n_t, for the first four-point step. The spatial wavelength and the period of the time oscillations are given by L_x and $\mathcal{T}_0$, respectively. In each case, the collision number interval is the same. Thick gray lines are nodal lines, the region indicated by a plus sign $(+)$ is the region where $\langle \delta q_{yj}^{(n)}/p_{yj}\rangle_t$ is positive, and the region indicated by a minus sign $(-)$ is the region where $\langle \delta q_{yj}^{(n)}/p_{yj}\rangle_t$ is negative. The phases in $[P3]$ and $[P4]$ differ from the phases in $[P1]$ and $[P2]$ by a simple shift of $\pi/2$ in the vertical (spatial) direction. The phases in $[P1]$ and $[P3]$ differ from the phases in $[P2]$ and $[P4]$ by a simple shift of $\pi/2$ in horizontal (time) direction.

half of the period of the oscillation corresponding to λ_{145}. These graphs, especially Fig. 9(b), are the most difficult graphs in which to recognize the wavelike structures in their three-dimensional plots, and in order to recognize the structures the contour plots given in the bottoms of these two three-dimensional plots may be helpful. In these contour plots we show mountain regions where $(\langle \delta q_{yj}^{(n)}/p_{yj}\rangle_t = 0.08)$ by dotted contour lines, and valley regions where $(\langle \delta q_{yj}^{(n)}/p_{yj}\rangle_t = -0.08)$ by dashed contour lines. The solid contour lines correspond to $\langle \delta q_{yj}^{(n)}/p_{yj}\rangle_t = 0$.

Now we consider the relationship between the quantities $\langle \delta q_{yj}^{(n)}/p_{yj}\rangle_t$ in the Lyapunov modes for the first four-point step. Figure 10 contains the contour plots of the quantity $\langle \delta q_{yj}^{(n)}/p_{yj}\rangle_t$ as a function of the normalized position $\langle q_{xj}\rangle_t/L_x$ and the collision number n_t for the first four-point step consisting of the Lyapunov exponents λ_{145}, λ_{144}, λ_{143}, and λ_{142}, over the same collision number interval [538 500,548 100]. Here, dotted lines, solid lines, and dashed lines correspond to $\langle \delta q_{yj}^{(n)}/p_{yj}\rangle_t = 0.08$, 0, and -0.08, respectively. It is clear that in these four graphs their spatial wavelengths (determined by L_x) and time-oscillating periods (determined by $\mathcal{T}_0$) are almost the same. (In this paper, we use the quantity $\mathcal{T}_0$ as the period in units of the particle-particle collision number, but we can convert it into the real time interval by multiplying by the mean free time, which is about 0.0243 for this system.) On the other hand, we can recognize that the position of the nodes of the spatial waves in graphs 10(a) and 10(b) as well as the nodes of the spatial waves in graphs 10(c) and 10(d) coincide with each other approximately, and the phase difference between the spatial waves in graphs 10(a) and 10(c) is approximately $\pi/2$. Besides, the node of the time oscillation in graphs 10(a) and 10(c) as well as the nodes of the time oscillation in graphs 10(b) and 10(d) coincide with each other approximately, and the phase difference between time oscillations in graphs 10(a) and 10(b) is about $\pi/2$. These points are summarized in Fig. 11, which is a schematic illustration of the phase relations amongst the time-oscillating wavelike structures for the quantity $\langle \delta q_{yj}^{(n)}/p_{yj}\rangle_t$. Here, the phases $[P1]$, $[P2]$, $[P3]$, and $[P4]$ correspond to those in Figs. 10(a), 10(b), 10(c), and 10(d), respectively. These observations suggest that the Lyapunov vector components $\delta q_{yj}^{[\tilde{n}(k)]}$, $\delta q_{yj}^{[\tilde{n}(k)-1]}$, $\delta q_{yj}^{[\tilde{n}(k)-2]}$, and $\delta q_{yj}^{[\tilde{n}(k)-3]}$ corresponding to the Lyapunov exponents for the kth four-point step can be expressed approximately as

$$
\begin{aligned}
&\{\delta q_{yj}^{[\tilde{n}(k)]}, \delta q_{yj}^{[\tilde{n}(k)-1]}, \delta q_{yj}^{[\tilde{n}(k)-2]}, \delta q_{yj}^{[\tilde{n}(k)-3]}\} \\
&\quad \approx \left\{ \tilde{\alpha}_k p_{yj} \cos\left(\frac{2\pi k}{L_x} q_{xj} + \tilde{\beta}_k\right) \cos\left(\frac{2\pi k}{\mathcal{T}_0} n_t + \tilde{\gamma}_k\right), \right. \\
&\qquad \tilde{\alpha}_k p_{yj} \cos\left(\frac{2\pi k}{L_x} q_{xj} + \tilde{\beta}_k\right) \sin\left(\frac{2\pi k}{\mathcal{T}_0} n_t + \tilde{\gamma}_k\right), \\
&\qquad \tilde{\alpha}_k p_{yj} \sin\left(\frac{2\pi k}{L_x} q_{xj} + \tilde{\beta}_k\right) \cos\left(\frac{2\pi k}{\mathcal{T}_0} n_t + \tilde{\gamma}_k\right), \\
&\qquad \left. \tilde{\alpha}_k p_{yj} \sin\left(\frac{2\pi k}{L_x} q_{xj} + \tilde{\beta}_k\right) \sin\left(\frac{2\pi k}{\mathcal{T}_0} n_t + \tilde{\gamma}_k\right) \right\}, \qquad (4)
\end{aligned}
$$

$j = 1,2,\ldots,N$, with constants $\tilde{\alpha}_k$, $\tilde{\beta}_k$, and $\tilde{\gamma}_k$. It should be emphasized that the level of agreement between Eq. (4) and the numerical results for the four-point steps is worse than the agreement between Eq. (3) and the numerical results for the two-point steps.

IV. QUASI-ONE-DIMENSIONAL SYSTEMS WITH A HARD-WALL BOUNDARY CONDITION

In this section, we consider quasi-one-dimensional systems with varied boundary conditions, replacing periodic by hard-wall boundary conditions in one or both directions. Given that there are two directions in which we can introduce the hard-wall boundary conditions, we consider three cases: (P,H), the case of periodic boundary conditions in the x direction and hard-wall boundary conditions in the y direction; (H,P), the case of hard-wall boundary conditions in the x direction and periodic boundary conditions in the y direction; and (H,H), the case of hard-wall boundary conditions in both the directions. Adopting the hard-wall boundary condition in a particular direction breaks the spatial translational invariance in that direction, so it allows us to discuss the role of momentum conservation in the stepwise structure

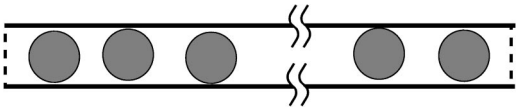

FIG. 12. A schematic illustration of a quasi-one-dimensional system with periodic boundary conditions in the x direction and hard-wall boundary conditions in the y direction, (P,H). The dashed line on the boundary represents periodic boundary conditions, and the solid line on the boundary represents hard-wall boundary conditions.

of the Lyapunov spectrum by comparing models having hard-wall boundary conditions with models having periodic boundary conditions. We will get different stepwise structures for the Lyapunov spectra in the above three cases compared with the previous case, and the investigation of the corresponding Lyapunov vectors allows us to relate and to categorize them.

In the systems with a hard-wall boundary condition, we should carefully choose the width L_x and the height L_y of the systems for meaningful comparisons between the results of different systems. It should be noted that in systems with pure periodic boundary conditions, the centers of particles can reach to the periodic boundaries, while in hard-wall boundary conditions the centers of particles can only reach within a distance R (the particle radius) of the hard-wall boundaries. In this sense, the effective region for particles to move in the system with hard-wall boundary conditions is smaller than that in the corresponding system with periodic boundary conditions, if we choose the same lengths L_x and L_y. In this section, the lengths L_x and L_y of the systems with a hard-wall boundary condition are chosen so that the effective region for a particle to move is the same as in the purely periodic boundary case considered in the preceding section, and are given by $(L_y,L_x)=(2R(1+10^{-6})+2R,1.5N(L_y-2R))$ in the case (P,H), $(L_y,L_x)=(2R(1+10^{-6}),1.5NL_y+2R)$ in the case (H,P), and $(L_y,L_x)=(2R(1+10^{-6})+2R,1.5N(L_y-2R)+2R)$ in the case (H,H). These choices of the lengths L_x and L_y also lead to almost the same mean free time for particle-particle collisions in the four different boundary condition cases. In the cases of (P,H) and (H,H) with this choice of the system width L_y, there is, in principle, space for the particle positions to interchange in the x direction [that is, strictly speaking these cases do not satisfy the second condition of Eq. (1)] but the space is extremely narrow (that is, $2R\times10^{-6}$) so that it is almost impossible for particle positions to actually be exchanged. Indeed, in our simulations no particle exchanges are observed.

A. The case of periodic boundary conditions in the x direction and hard-wall boundary conditions in the y direction

The first case is the quasi-one-dimensional system with periodic boundary conditions in the x direction and with hard-wall boundary conditions in the y direction [the boundary case (P,H)]. A schematic illustration of this system is given in Fig. 12 in which periodic boundary conditions and hard-wall boundary conditions are represented as dashed lines and bold solid lines, respectively.

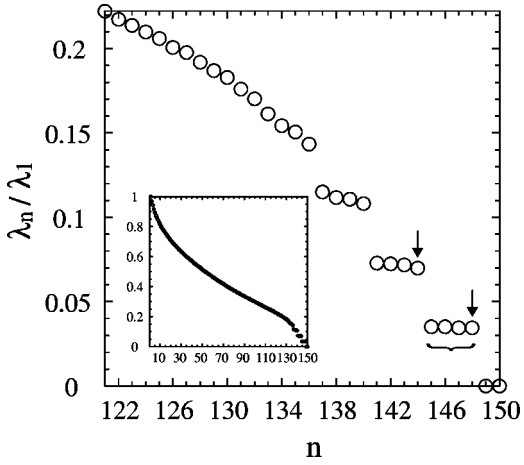

FIG. 13. Stepwise structure of the Lyapunov spectrum normalized by the maximum Lyapunov exponent for the quasi-one-dimensional system with periodic boundary conditions in the x direction and hard-wall boundary conditions in the y direction. Inset: Full scale of the normalized Lyapunov spectrum.

Figure 13 is the Lyapunov spectrum normalized by the maximum Lyapunov exponent $\lambda_1\approx1.30$ for this system. In this figure, we showed a small positive region of the Lyapunov spectrum including its stepwise structures, while the full scale of the positive branch of the Lyapunov spectrum is shown in the inset. In this system the y component of the total momentum is not conserved because of the hard-wall boundary conditions in the y direction, so there are only four zero-Lyapunov exponents in this system. This figure shows clearly that the steps of the Lyapunov spectrum consist of four-point steps only, and there is no two-point step in the Lyapunov spectrum which appears in the model discussed in the preceding section. Besides, we cannot recognize a wavelike structure in the graph of Lyapunov vector components $\langle \delta q_{yj}^{(n)} \rangle$ as a function of the position $\langle q_{xj} \rangle$ (the graph $[Ts]$) in this model. A comparison of this fact with results in the previous model suggests that the two-point step of the Lyapunov spectrum in the preceding section should be strongly connected to the conservation of the y component of the total momentum.

We consider a relation between the four-point steps in the model of this section and in the model of the preceding section by investigating the graph of the quantity $\langle \delta q_{yj}^{(n)}/p_{yj} \rangle_t$ as a function of the normalized position $\langle q_{xj} \rangle_t/L_x$ and the collision number n_t (the graph $[Tt]$). (Note that in this paper we use n_t as the collision, number of particle-particle collisions which does not include particle-wall collisions, in order to make the collision number n_t of the four different boundary condition cases comparable.) Figure 14 presents graphs corresponding to the Lyapunov exponent λ_{148} in the first four-point step [Fig. 14(a)] and the Lyapunov exponent λ_{144} in the second four-point step [Fig. 14(b)], which are indicated by arrows in Fig. 13, using the same collision number interval [390 600,396 000]. The wavelike structures of these graphs have a wavelength $1/i$ for the ith four-point steps. The time-oscillating period corresponding to the Lyapunov exponent λ_{148} is almost the same as the period $\mathcal{T}_0$ of the first

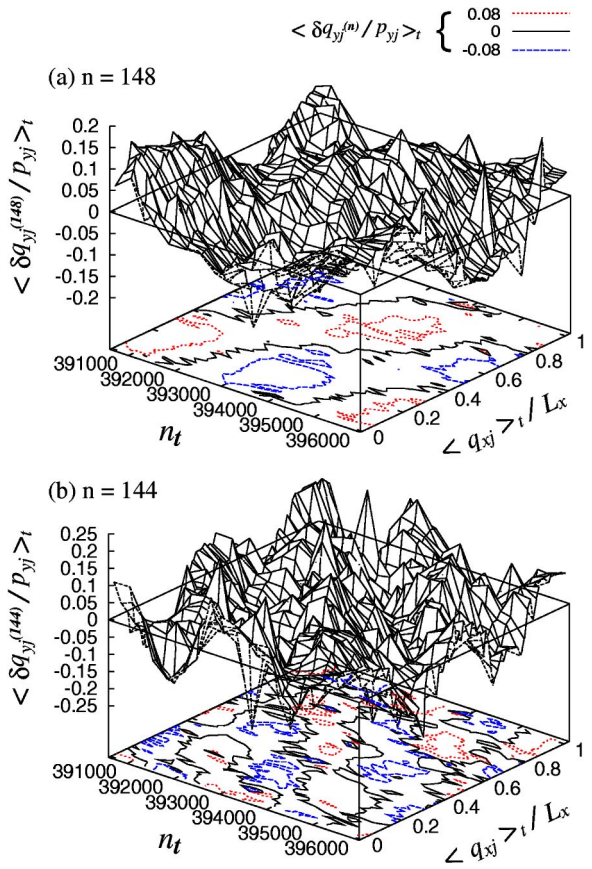

FIG. 14. Local time-averaged quantities $\langle \delta q_{yj}^{(n)}/p_{yj}\rangle_t$ as functions of the normalized position $\langle q_{xj}\rangle_t/L_x$ and the collision number n_t corresponding to the Lyapunov exponents λ_{148} and λ_{144} in the same collision number interval [390 600,396 000]. The system is the quasi-one-dimensional system (P,H) with periodic boundary conditions in the x direction and hard-wall boundary conditions in the y direction, and the corresponding Lyapunov exponents are indicated by arrows in Fig. 13. Contour plots on the bottoms of these three-dimensional plots are given by dotted lines, solid lines, and dashed lines corresponding to the values $\langle \delta q_{yj}^{(n)}/p_{yj}\rangle_t = 0.08$, 0, and -0.08, respectively.

four-point steps of the previous model, and is approximately twice as long as the time-oscillating period in the Lyapunov exponent λ_{144} of this model. These features are common with the four-point steps in the models of the preceding section, suggesting that the four-point steps of the Lyapunov spectrum in this model correspond to the four-point steps in the model of the preceding section. We can also show that the quantities $\langle \delta q_{yj}^{(n)}/p_{yj}\rangle_t$ corresponding to the zero-Lyapunov exponents λ_{150} and λ_{149} are approximately constants as functions of $\langle q_{xj}\rangle_t$ and n_t.

Now we proceed to investigate the graph of the quantities $\langle \delta q_{yj}^{(n)}/p_{yj}\rangle_t$ corresponding to the Lyapunov exponents in the same four-point steps of the Lyapunov spectrum. Figure 15 shows the contour plots of these quantities as functions of the normalized position $\langle q_{xj}\rangle_t/L_x$ and the collision number n_t, corresponding to the first four-point step consisting of the Lyapunov exponents λ_{148}, λ_{147}, λ_{146}, and λ_{145}, in the same collision number interval [385 800,396 000]. The corresponding Lyapunov exponents are indicated by the brace under circles in Fig. 13. In this case, the contour lines of $\langle \delta q_{yj}^{(n)}/p_{yj}\rangle_t = 0$ seem to be slanting, but if we pay attention to the mountain regions and the valley regions in these graphs then we can realize that the structure of these four graphs are similar to the contour plots of the four graphs in Fig. 10 for the previous model. Therefore, the phase relations among the time-oscillating wavelike structures of the quantity $\langle \delta q_{yj}^{(n)}/p_{yj}\rangle_t$ can be summarized in the schematic illustration given in Fig. 11 such as in the previous model. This suggests an approximate expression for the Lyapunov vector components given by Eq. (4), for Lyapunov vector components $\delta q_{yj}^{(n)}$ corresponding to the Lyapunov exponents of the four-point steps in this model.

B. The case of hard-wall boundary conditions in the x direction and periodic boundary conditions in the y direction

As the next system, we consider a quasi-one-dimensional system with hard-wall boundary conditions in the x direction and periodic boundary conditions in the y direction [the boundary case (H,P)]. A schematic illustration of such a system is given in Fig. 16 with solid lines for the hard-wall boundary conditions and dashed lines for the periodic boundary conditions.

In this system, the x component of the total momentum is not conserved, so the total number of the zero-Lyapunov exponents is 4. Figure 17 is a small positive region of the Lyapunov spectrum normalized by the maximum Lyapunov exponent $\lambda_1 \approx 1.30$, including its stepwise structure, while its whole positive part of the Lyapunov spectrum is given in the inset. The stepwise structure of the Lyapunov spectrum is clearly different from the model of Sec. IV A, and consists of two-point steps interrupted by isolated single-Lyapunov exponents. (We call the isolated single-Lyapunov exponents interrupting the two-point steps ''one-point steps'' from now on, partly because they are connected to the two-point steps in the model of Sec. III as will be shown in this section.) As discussed in Sec. III, the Lyapunov spectrum for the model with periodic boundary conditions in both directions has two-point steps and four-point steps, and it is remarkable that adopting hard-wall boundary conditions in the x direction and destroying the total momentum conservation in this direction halve the step widths of both kinds of steps.

Figure 18 shows the graphs of the time-averaged Lyapunov vector components $\langle \delta q_{yj}^{(n)}\rangle$ as functions of the normalized position $\langle q_{xj}\rangle/L_x$ (the mode $[Ts]$), corresponding to the one-point steps. We can clearly recognize wavelike structures in these graphs, and in this sense the one-point steps in this model should be strongly related to the two-point steps in the model of Sec. III. The Lyapunov exponents accompanying wavelike structure of this kind of graphs are shown in Fig. 17 as black-filled circle dots, meaning that they are the one-point steps. In Fig. 17, we also filled the circle symbols with gray for one of the zero-Lyapunov exponents in which the graph of the Lyapunov vector components $\langle \delta q_{yj}^{(n)}\rangle$ as a function of the position $\langle q_{xj}\rangle$ is constant approximately. However, it is important to note that the wavelength of the wave corresponding to the ith one-point step in this model is $2/i$, not $1/i$ as in the model of Sec. III. We fitted the graphs

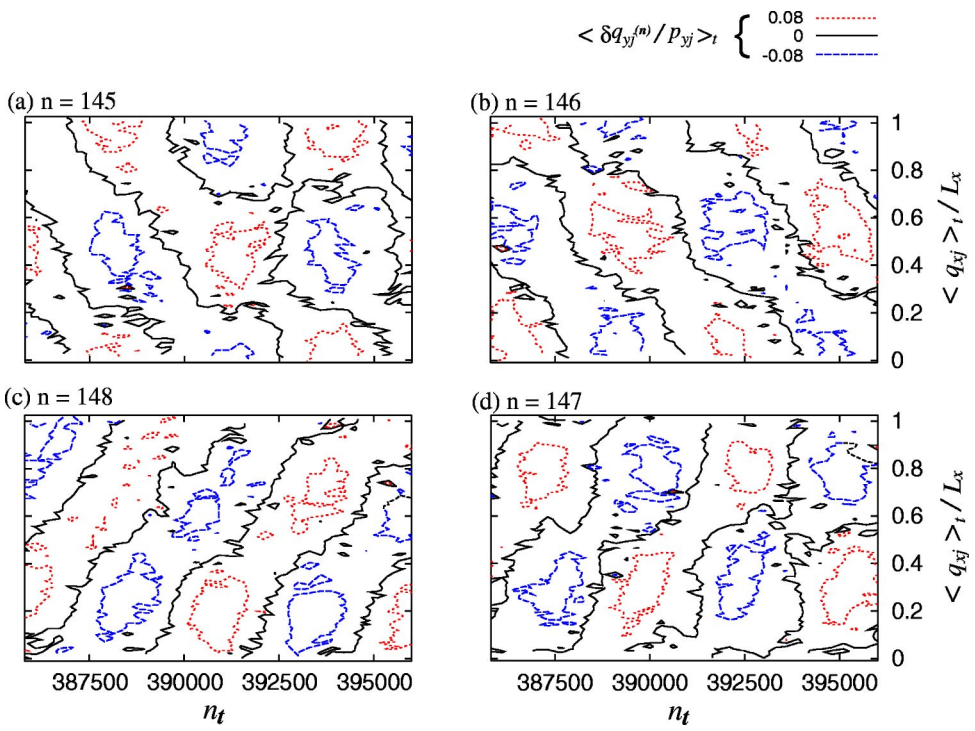

FIG. 15. Contour plots of the time-averaged quantities $\langle \delta q_{yj}^{(n)}/p_{yj}\rangle_t$ as functions of the normalized position $\langle q_{xj}\rangle_t/L_x$ and the collision number n_t corresponding to the first four-point step consisting of the Lyapunov exponents λ_{148}, λ_{147}, λ_{146}, and λ_{145}, in the same collision number interval [385 800,396 000]. The system is the quasi-one-dimensional system (P,H) with periodic boundary conditions in the x direction and hard-wall boundary conditions in the y direction, and the corresponding Lyapunov exponents are indicated by the brace under circles in Fig. 13. Here dotted lines, solid lines, and dashed lines correspond to the values $\langle \delta q_{yj}^{(n)}/p_{yj}\rangle_t = 0.08$, 0, and -0.08, respectively.

corresponding to the Lyapunov exponents λ_{149}, λ_{148}, λ_{145}, and λ_{142} by the functions $y=\alpha_{149}, \alpha_{148}\cos(\pi x+\beta_{148}), \alpha_{145}\cos(2\pi x+\beta_{145}), \alpha_{142}\cos(3\pi x+\beta_{142})$, respectively, with α_n and β_n as fitting parameters. Here, the values of the fitting parameters were found to be $\alpha_{149}=0.115\,47$, $(\alpha_{148},\beta_{148})=(0.162\,13,-0.008\,977\,8)$, $(\alpha_{145},\beta_{145})=(-0.162\,02,-0.010\,07)$, and $(\alpha_{142},\beta_{142})=(-0.159\,45,0.008\,914\,8)$. The graphs are very nicely fitted by a constant or the sinusoidal functions, and lead to the form

$$\delta q_{yj}^{[n(k)]} \approx \alpha_k' \cos\left(\frac{\pi k}{L_x} q_{xj} + \beta_k'\right), \tag{5}$$

$j=1,2,\ldots,N$, of the Lyapunov vector component $\delta q_{yj}^{[n(k)]}$ corresponding to the Lyapunov exponents $\lambda_{n(k)}$ in the kth one-point step with constants α_k' and β_k'.

Now we investigate the remaining steps, namely, the two-point steps of the Lyapunov spectrum. Corresponding to these two-point steps of the Lyapunov spectrum, the graphs of the quantity $\langle \delta q_{yj}^{(n)}/p_{yj}\rangle_t$ as functions of the normalized position $\langle q_{xj}\rangle_t/L_x$ and the collision number n_t (the mode $[Tt]$) show spatial wavelike structures oscillating in time. It is shown in Fig. 19 for those graphs corresponding to

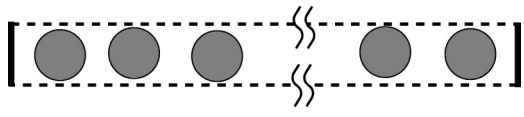

FIG. 16. A schematic illustration of a quasi-one-dimensional system (H,P) with hard-wall boundary conditions in the x direction and periodic boundary conditions in the y direction. The solid lines for the boundary represent hard-wall boundary conditions, and dashed lines represent periodic boundary conditions.

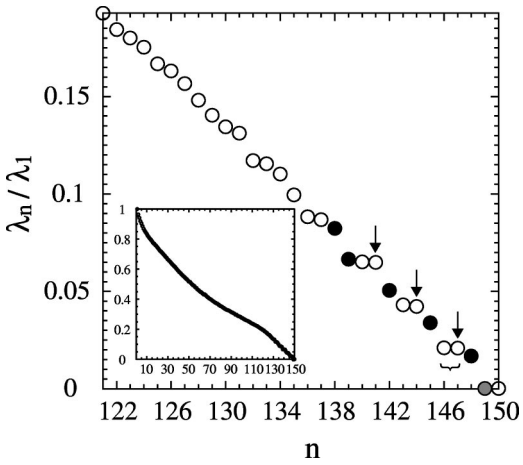

FIG. 17. Stepwise structure of the Lyapunov spectrum normalized by the maximum Lyapunov exponent for the quasi-one-dimensional system with hard-wall boundary conditions in the x direction and periodic boundary conditions in the y direction. Inset: Full scale of the normalized Lyapunov spectrum. The circle dots filled by black (gray) are the Lyapunov exponents accompanying wavelike structure (a constant behavior) of the Lyapunov vector components $\langle \delta q_{yj}^{(n)}\rangle$ partly shown in Fig. 18.

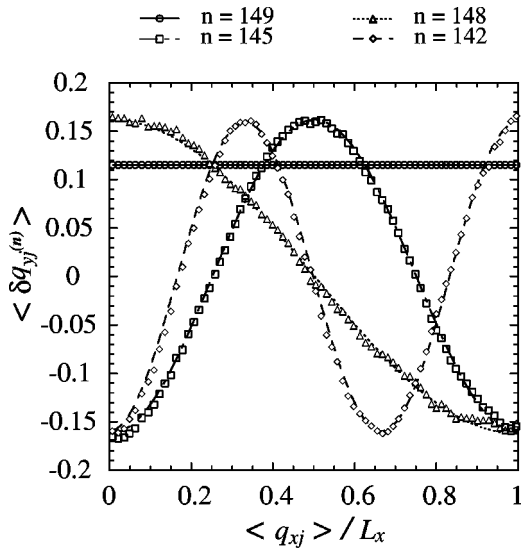

FIG. 18. Time-averaged Lyapunov vector components $\langle \delta q_{yj}^{(n)} \rangle$ corresponding to the Lyapunov exponents λ_{149}, λ_{148}, λ_{145}, and λ_{142}, as functions of the time-averaged particle position $\langle q_{xj} \rangle / L_x$ normalized by the system length L_x. The system is the quasi-one-dimensional system (H,P) with hard-wall boundary conditions in the x direction and periodic boundary conditions in the y direction, and the corresponding Lyapunov exponents are shown as the black- and gray-filled circles in Fig. 17. The numerical data are fitted by either a constant or sinusoidal function.

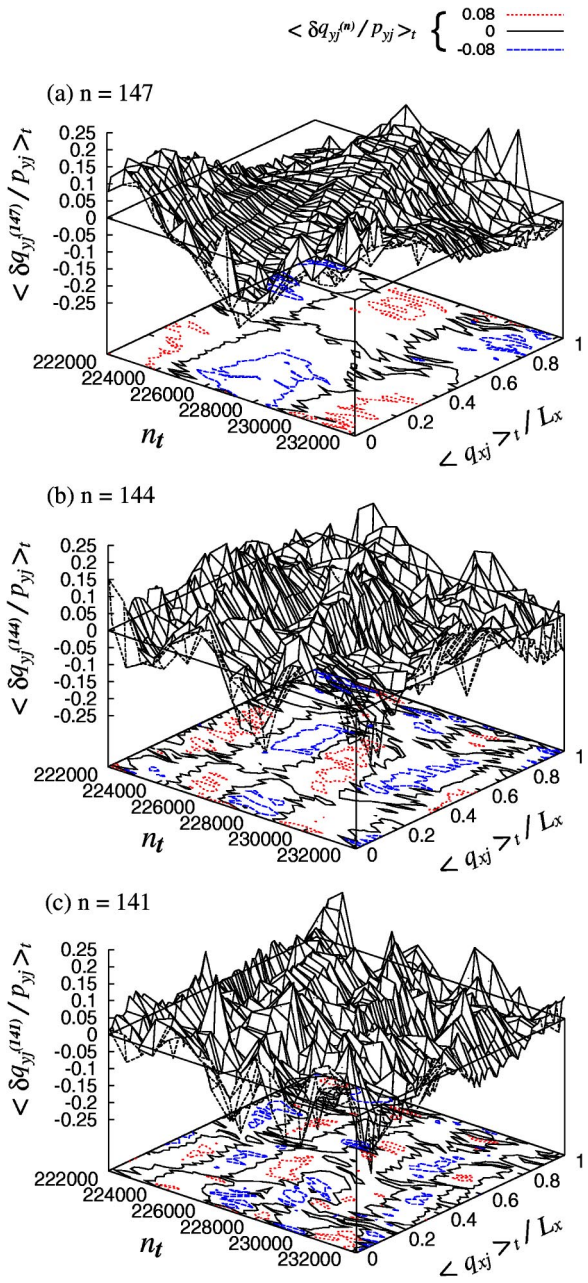

FIG. 19. Local time-averaged quantities $\langle \delta q_{yj}^{(n)} / p_{yj} \rangle_t$ as functions of the normalized position $\langle q_{xj} \rangle_t / L_x$ and the collision number n_t corresponding to the Lyapunov exponents λ_{147}, λ_{144}, and λ_{141}, in the same collision number interval [222 000,232 200]. The system is the quasi-one-dimensional system (H,P) with hard-wall boundary conditions in the x direction and periodic boundary conditions in the y direction, and the corresponding Lyapunov exponents are indicated by arrows in Fig. 17. Contour plots on the bottoms of these three-dimensional plots are given by dotted lines, solid lines, and dashed lines corresponding to the values $\langle \delta q_{yj}^{(n)} / p_{yj} \rangle_t = 0.08$, 0, and -0.08, respectively.

Lyapunov exponents (indicated by arrows in Fig. 17) in different two-point steps, in the same collision number interval [222 000,232 200]. The spatial wavelength of the waves corresponding to the ith two-point step is $2/i$, which is twice as long as the wavelength of waves of the four-point steps in the models in Sec. III and the preceding section. The period of time oscillation of the wave corresponding to the ith two-point step of the Lyapunov spectrum is approximately given by $\mathcal{T}_0'/i$ with a constant $\mathcal{T}_0'$. The graph corresponding to one of the zero-Lyapunov exponents, namely λ_{150}, is almost constant.

It is important to note the relation between the time-oscillating period $\mathcal{T}_0$ of the preceding two models and the time-oscillating period $\mathcal{T}_0'$ of the model in this section. Noting that in Figs. 9(a), 14(a), and 19(a) we plotted about one period of the time oscillation of the wavelike structures of the quantities $\langle \delta q_{yj}^{(n)} / p_{yj} \rangle_t$ in the collision time intervals [543 000,548 100], [390 600,396 000], and [222 000,232 200], respectively, we can get an approximate relation $\mathcal{T}_0' \approx 2\mathcal{T}_0$.

The next problem is to investigate the graphs of the quantities $\langle \delta q_{yj}^{(n)} / p_{yj} \rangle_t$ as a function of the position $\langle q_{xj} \rangle_t$ and the collision number n_t in the same two-point step of the Lyapunov spectrum. Figure 20 shows the contour plots of such graphs for the first two-point step consisting of the Lyapunov exponents λ_{147} and λ_{146}, which is indicated by a brace under circles in Fig. 17, in the same collision number interval [212 400,232 200]. It should be noted that the positions of the nodes of two spatial waves belonging to the same two-point step almost coincide with each other. However, the phases of the time oscillations of the amplitudes of the waves are shifted by about $\pi/2$ with each other. The phase relations of graphs 20(a) and 20(b) are visualized in the schematic illustration given in Fig. 21 of the time-oscillating wavelike structures of the quantities $\langle \delta q_{yj}^{(n)} / p_{yj} \rangle_t$ corresponding to the

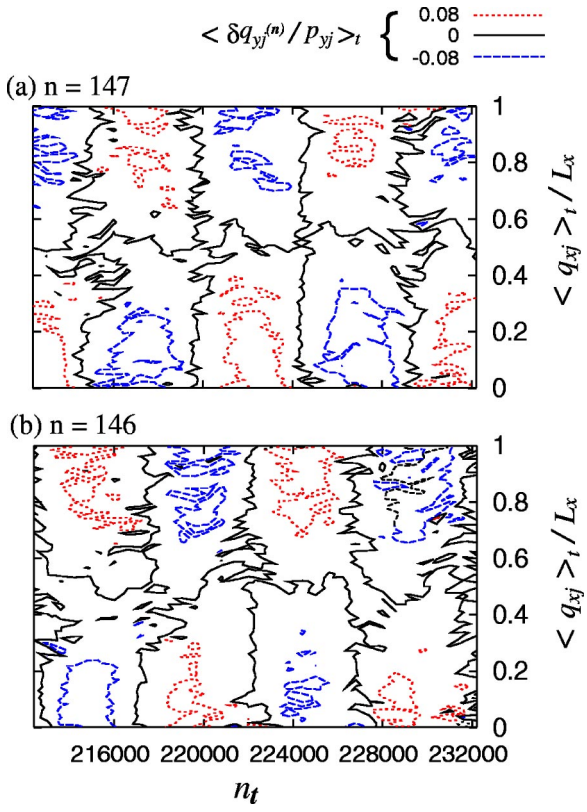

FIG. 20. Contour plots of the local time-averaged quantities $\langle \delta q_{yj}^{(n)}/p_{yj}\rangle_t$ as functions of the normalized position $\langle q_{xj}\rangle_t/L_x$ and the collision number n_t corresponding to the first two-point step consisting of the Lyapunov exponents λ_{147} and λ_{146}, in the same collision number interval [212 400,232 200]. The system is the quasi-one-dimensional system (H,P) with hard-wall boundary conditions in the x direction and periodic boundary conditions in the y direction, and the corresponding Lyapunov exponents are indicated by the brace under circles in Fig. 17. Here dotted lines, solid lines, and dashed lines correspond to the values $\langle \delta q_{yj}^{(n)}/p_{yj}\rangle_t = 0.08$, 0, and -0.08, respectively.

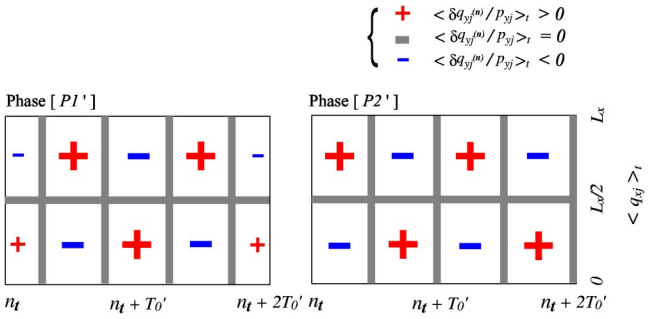

FIG. 21. Schematic illustration of the phase relations among the time-oscillating wavelike structures of the quantities $\langle \delta q_{yj}^{(n)}/p_{yj}\rangle_t$ as functions of the position $\langle q_{xj}\rangle_t$ and the collision number n_t, corresponding to the first two-point step in the same collision number interval. Thick gray lines mean node lines, the region indicated by a plus sign (+) is the region where the quantity $\langle \delta q_{yj}^{(n)}/p_{yj}\rangle_t$ is positive, and the region indicated by a minus sign (−) is the region where the quantity $\langle \delta q_{yj}^{(n)}/p_{yj}\rangle_t$ is negative. The phase of $[P1']$ is shifted in time from the phase of $[P2']$ by $\pi/2$.

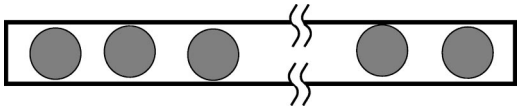

FIG. 22. A schematic illustration of a quasi-one-dimensional system (H,H) with hard-wall boundary conditions in both directions. The solid line on the boundary represents hard-wall boundary conditions.

first two-point step in the same collision number interval. Here the phases $[P1']$ and $[P2']$ correspond to Figs. 20(a) and 20(b), respectively. A similar investigation of the Lyapunov vectors shows that the time-oscillating wavelike structures for the second two-point steps are like those of phases $[P1]$ and $[P2]$ of Fig. 11 except that the period $\mathcal{T}_0$ in Fig. 11 should be replaced with the oscillating period $\mathcal{T}_0'$ of this model. These results suggest that the two-point steps in this model correspond to the four-point steps in the models of Secs. IV A and III, except for differences in the values of their wavelengths and time-oscillating periods. After all we get a conjecture that the Lyapunov vector components $\delta q_{yj}^{[\tilde{n}(k)]}$ and $\delta q_{yj}^{[\tilde{n}(k)-1]}$ corresponding to the Lyapunov exponents constructing the kth two-point step are approximately expressed as

$$\{\delta q_{yj}^{[\tilde{n}(k)]}, \delta q_{yj}^{[\tilde{n}(k)-1]}\} \approx \left\{ \tilde{\alpha}_k' p_{yj} \cos\left(\frac{\pi k}{L_x} q_{xj} + \tilde{\beta}_k'\right) \cos\left(\frac{\pi k}{\mathcal{T}_0} n_t + \tilde{\gamma}_k'\right), \tilde{\alpha}_k' p_{yj} \cos\left(\frac{\pi k}{L_x} q_{xj} + \tilde{\beta}_k'\right) \sin\left(\frac{\pi k}{\mathcal{T}_0} n_t + \tilde{\gamma}_k'\right) \right\}, \quad (6)$$

$j=1,2,\ldots,N$ with constants $\tilde{\alpha}_k'$, $\tilde{\beta}_k'$, and $\tilde{\gamma}_k'$, noting the time-oscillating period $\mathcal{T}_0' \approx 2\mathcal{T}_0$.

C. The case of hard-wall boundary conditions in both directions

The last model is the case of hard-wall boundary conditions in both directions [the boundary case (H,H)]. A schematic illustration of this system is given in Fig. 22 in which the solid line of the boundary means to take hard-wall boundary conditions.

A small positive region of the Lyapunov spectrum normalized by the maximum Lyapunov exponent $\lambda_1 \approx 1.29$ is given in Fig. 23. The graph for the full scale of the positive branch of the normalized Lyapunov spectrum is also given in the inset of this figure. In this system the total momentum is not conserved anymore, and the total number of zero-Lyapunov exponents is 2. The stepwise structure of the Lyapunov spectrum consists of two-point steps only. In this model, a wavelike structure in the Lyapunov vector component $\langle \delta q_{yj}^{(n)}\rangle$ as a function of the position $\langle q_{xj}\rangle$ (the mode $[Ts]$) is not observed.

Figure 24 shows the graphs of the quantities $\langle \delta q_{yj}^{(n)}/p_{yj}\rangle_t$ as functions of the normalized position $\langle q_{xj}\rangle_t/L_x$ and the collision number n_t (the mode $[Tt]$), corresponding to the Lyapunov exponents λ_{149}, λ_{147}, and λ_{145}, using the same

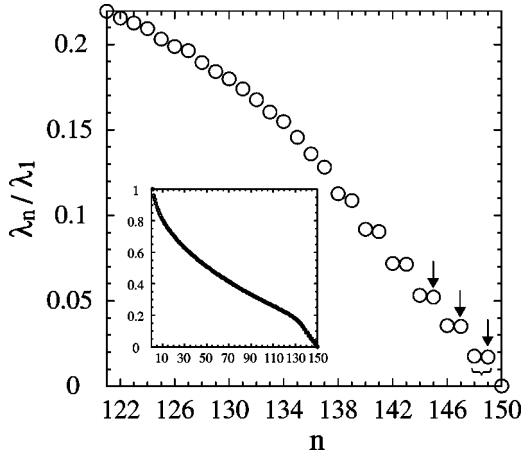

FIG. 23. Stepwise structure of the Lyapunov spectrum normalized by the maximum Lyapunov exponent for a quasi-one-dimensional system with hard-wall boundary conditions in both directions. Inset: Full scale of the normalized Lyapunov spectrum.

collision number interval [235 200,246 000]. The corresponding Lyapunov exponents are indicated by arrows in Fig. 23. This figure for the two-point steps of the Lyapunov spectrum shows a similar wavelike structure to the wavelike structure of the quantities $\langle \delta q_{yj}^{(n)}/p_{yj}\rangle_t$ in the model of Sec. IV B, although one may think that fluctuations of these graphs in this model are much smaller than in the previous model. This suggests that the two-point steps of the Lyapunov spectrum in Fig. 23 are similar to the two-point steps in the model of Sec. IV B. The wavelength of the spatial waves and the periods of the time oscillations corresponding to the ith two-point step are $2/i$ and $\mathcal{T}_0'/i$, respectively, and the time-oscillating period of the first two-point step is given approximately by the same period $\mathcal{T}_0'$ ($\approx 2\mathcal{T}_0$) as in the model of Sec. IV B. It may also be noted that this kind of graph corresponding to the zero-Lyapunov exponent λ_{150} is almost constant.

Figure 25 shows the contour plots of the quantities $\langle \delta q_{yj}^{(n)}/p_{yj}\rangle_t$ as functions of the normalized position $\langle q_{xj}\rangle_t/L_x$ and the collision number n_t corresponding to the Lyapunov exponents λ_{149} and λ_{148} in the first two-point step of the Lyapunov spectrum in the same collision number interval [223 800,246 000]. The corresponding Lyapunov exponents are indicated by the brace under circles in Fig. 23. Similarly to the previous model, the nodes of two spatial waves corresponding to the same two-point step almost coincide with each other, and the phase of the time oscillation of the wave amplitudes is shifted by about $\pi/2$. This also says that the phase relations of graphs 25(a) and 25(b) are the same type as the phase relations $[P1']$ and $[P2']$ in Fig. 21. In a similar way, we can see that the time-oscillating wavelike structures for the second two-point steps of the Lyapunov spectrum for this model are like the phases $[P1]$ and $[P2]$ of Fig. 11 by replacing the period $\mathcal{T}_0$ of Fig. 11 with the time-oscillating period $\mathcal{T}_0' \approx 2\mathcal{T}_0$ of this model. These suggest an approximate expression for the Lyapunov vector components given by Eq. (6), for Lyapunov vector components $\delta q_{yj}^{(n)}$ corresponding to the nth Lyapunov exponents of the kth two-point steps in this model. The fact that the only difference between the model in this section and the model in Sec. IV B is the boundary conditions in the y direction suggests that the one-point steps of the model in Sec. IV B come from the conservation of the y component of the total momentum.

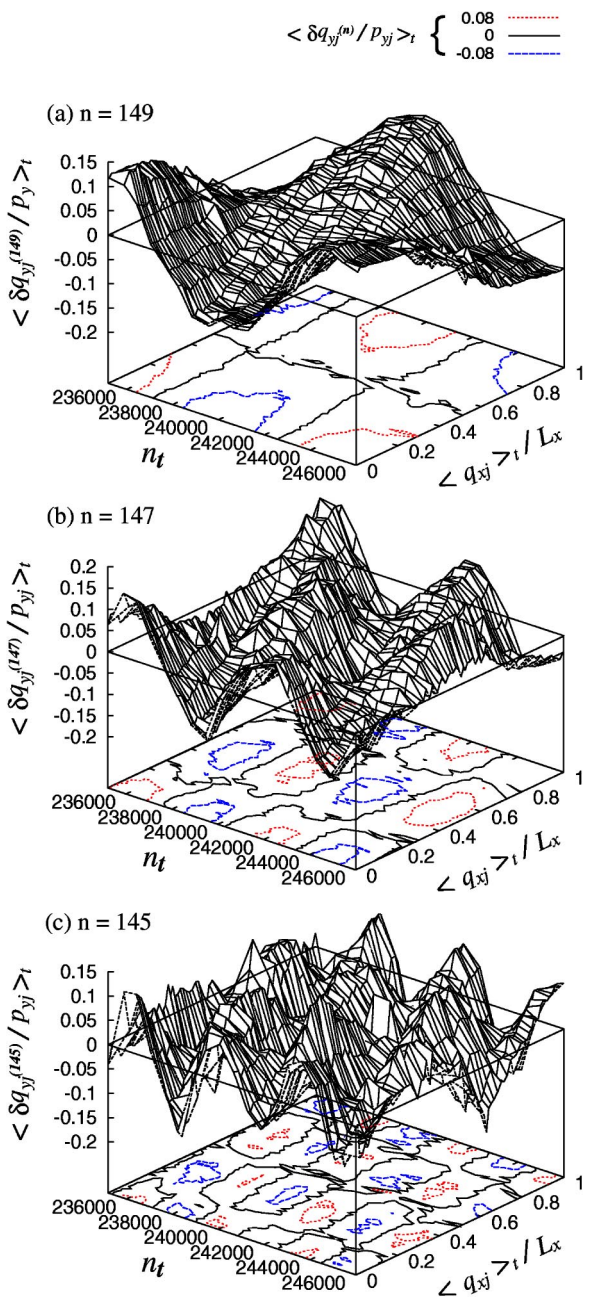

FIG. 24. Local time-averaged quantities $\langle \delta q_{yj}^{(n)}/p_{yj}\rangle_t$ as functions of the normalized position $\langle q_{xj}\rangle_t/L_x$ and the collision number n_t corresponding to the Lyapunov exponents λ_{149}, λ_{147}, and λ_{145}, in the same collision number interval [235 200,246 000]. The system is the quasi-one-dimensional system (H,H) with hard-wall boundary conditions in both directions, and the corresponding Lyapunov exponents are indicated by arrows in Fig. 23. Contour plots on the bottoms of these three-dimensional plots are given by dotted lines, solid lines, and dashed lines corresponding to the values $\langle \delta q_{yj}^{(n)}/p_{yj}\rangle_t = 0.08$, 0, and -0.08, respectively.

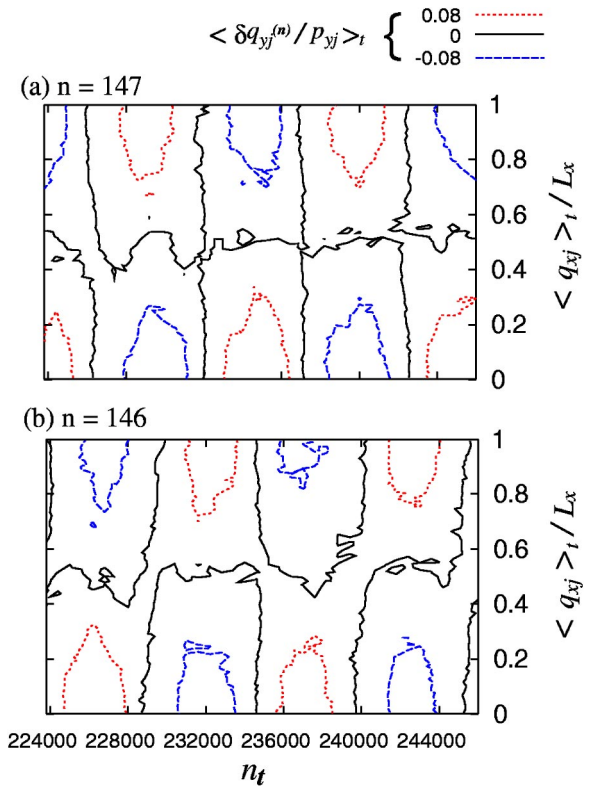

FIG. 25. Contour plots of the local time-averaged quantities $\langle \delta q_{yj}^{(n)}/p_{yj}\rangle_t$ as functions of the normalized position $\langle q_{xj}\rangle_t/L_x$ and the collision number n_t corresponding to the first two-point step consisting of the Lyapunov exponents λ_{149} and λ_{148} using the same collision number interval [223 800,246 000]. The system is the quasi-one-dimensional system (H,H) with hard-wall boundary conditions in both directions, and the corresponding Lyapunov exponents are indicated by the brace under circles in Fig. 23. Here, dotted lines, solid lines, and dashed lines correspond to the values $\langle \delta q_{yj}^{(n)}/p_{yj}\rangle_t = 0.08$, 0, and -0.08, respectively.

V. CONCLUSION AND REMARKS

In this paper, we have discussed numerically the stepwise structure of the Lyapunov spectra and its corresponding wavelike structures for the Lyapunov vectors in many-hard-disk systems. We concentrated on the quasi-one-dimensional system whose shape is a very narrow rectangle that does not allow exchange of disk positions. In the quasi-one-dimensional system, we can get a stepwise structure of the Lyapunov spectrum in a relatively small system, for example, even in a ten-particle system, whereas a fully two-dimensional system would require many more particles. In such a system, we have considered the following two problems: (a) How does the stepwise structure of the Lyapunov spectra depend on boundary conditions such as periodic boundary conditions and hard-wall boundary conditions? (b) How can we categorize the stepwise structure of the Lyapunov spectra using the wavelike structure of the corresponding Lyapunov vectors? To consider problem (a) also means to investigate the effects of the loss of spatial translational invariance on the stepwise structure of the Lyapunov spectra. In this paper, we considered four types of the boundary conditions; (P,P), purely periodic boundary conditions; (P,H), periodic boundary conditions in the x direction and hard-wall boundary conditions in the y direction; (H,P), hard-wall boundary conditions in the x direction and periodic boundary conditions in the y direction; and (H,H), purely hard-wall boundary conditions, in a system of rectangular shape where we took the y direction as the narrow direction. With each boundary case, we obtained different stepwise structures of the Lyapunov spectra. For each boundary condition, we also considered graphs of the following two modes; $[Ts]$, the y component $\delta q_{yj}^{(n)}$ of the spatial coordinate part of the Lyapunov vector of the jth particle corresponding to the Lyapunov exponent λ_n as a function of the x component q_{xj} of the spatial component of the jth particle, and $[Tt]$, the quantity $\delta q_{yj}^{(n)}/p_{yj}$ with the y component p_{yj} of the momentum coordinate of the jth particle as a function of the position q_{xj} and the collision number n_t. These quantities $\delta q_{yj}^{(n)}$ and $\delta q_{yj}^{(n)}/p_{yj}$ give constant values in some of the zero-Lyapunov exponents, at least approximately. We found that the steps of the Lyapunov spectra accompany a wavelike structure in the quantity $\delta q_{yj}^{(n)}$ or $\delta q_{yj}^{(n)}/p_{yj}$, depending on the kind of steps of the Lyapunov spectra. A time-dependent oscillating behavior appears in the wavelike structure of the quantity $\delta q_{yj}^{(n)}/p_{yj}$, whereas the wavelike structure of the quantity $\delta q_{yj}^{(n)}$ is essentially stationary. Fluctuations of these quantities $\delta q_{yj}^{(n)}$ and $\delta q_{yj}^{(n)}/p_{yj}$ disturb their clear oscillatory structures, so we took a time average of these quantities (a local time average for the quantity $\delta q_{yj}^{(n)}/p_{yj}$ because of its time-oscillating behavior, and a longer time-average for the quantity $\delta q_{yj}^{(n)}$ because it is much more stationary in time than the quantity $\delta q_{yj}^{(n)}/p_{yj}$) to get their dominant wavelike structures. In Table I, we summarize our results about a categorization of the stepwise structures of the Lyapunov spectra by the wavelike structures of the Lyapunov vectors in the four boundary cases (P,P), (P,H), (H,P), and (H,H). In Lyapunov exponents in each step of the Lyapunov spectra, the wavelike structures of the quantity $\delta q_{yj}^{(n)}$ or $\delta q_{yj}^{(n)}/p_{yj}$ are approximately orthogonal to each other in space [in the sense of Eq. (3)], in space and time [in the sense of Eq. (4)], or in time [in the sense of Eq. (6)], and this fact suggests that the wavelike structures of these quantities are sufficient to categorize the stepwise structure of the Lyapunov spectra in the quasi-one-dimensional systems considered here.

Hard-wall boundary conditions may be emulated in an infinite system by reflecting the positions and velocities of all particles at each hard wall. The infinite system modes that survive are those that satisfy the reflection symmetries. For translational modes this requires combinations that produce standing waves, with nodes at the walls for modes with deviations normal to the wall, and antinodes for modes with deviations parallel to the wall, if the modes of the entire system are connected smoothly at the walls. Further, for hard-wall systems the number of k values allowed is doubled because half periods are also allowed. In this way, we may begin developing a theoretical picture that predicts the types of Lyapunov modes and the range of k values for which these modes are stable. Although this is the ultimate goal of these numerical investigations, the complete theoretical description remains an open problem.

TABLE I. The categorization of the stepwise structures of the Lyapunov spectra and the associated wavelike structures of the Lyapunov vectors in two-dimensional rectangular systems with the four boundary cases considered in this paper. The case (P,P) is the purely periodic boundary case (Sec. III) represented in Fig. 6, the case (P,H) is the periodic boundary condition in the x direction and hard-wall boundary condition in the y direction (Sec. IV A) represented in Fig. 12, the case (H,P) is the hard-wall boundary condition in the x direction and periodic boundary condition in the y direction (Sec. IV B) represented in Fig. 16, and the case (H,H) is the purely hard-wall boundary condition (Sec. IV C) represented in Fig. 22. Here we took the y direction as the narrow direction of the rectangle and the x direction as the longer orthogonal direction. The mode $[Ts]_j$ is the stationary transverse Lyapunov mode appearing in $\delta q_{yj}^{(n)}$ as a function of q_{xj}, and the mode $[Tt]_j$ is a spatial wavelike structure with a time oscillation in $\delta q_{yj}^{(n)}/p_{yj}$ as a function of q_{xj} and time. The suffices $j=1,2,\ldots$ in the label of modes $[Ts]_j$ and $[Tt]_j$ are the step numbers of the sequence in the Lyapunov spectra. In this table, $\mathcal{S}$ is the number of points in the step (or the number of the zero-Lyapunov exponents in the line specified by the label "$\lambda_n=0$"), $\mathcal{L}$ is the wavelength of spatial wavelike structure, and $\mathcal{T}$ is the period of time oscillation of the wave, L_x is the length of the quasi-one-dimensional rectangle, and $\mathcal{T}_0$ is constant.

	(P,P)			(P,H)			(H,P)			(H,H)		
Mode	$\mathcal{S}$	$\mathcal{L}$	$\mathcal{T}$	$\mathcal{S}$	$\mathcal{L}$	$\mathcal{T}$	$\mathcal{S}$	$\mathcal{L}$	$\mathcal{T}$	$\mathcal{S}$	$\mathcal{L}$	$\mathcal{T}$
$\lambda_n=0$	6			4			4			2		
$[Ts]_1$	2	$L_x/1$					1	$2L_x/1$				
$[Tt]_1$	4	$L_x/1$	$\mathcal{T}_0/1$	4	$L_x/1$	$\mathcal{T}_0/1$	2	$2L_x/1$	$2\mathcal{T}_0/1$	2	$2L_x/1$	$2\mathcal{T}_0/1$
$[Ts]_2$	2	$L_x/2$					1	$2L_x/2$				
$[Tt]_2$	4	$L_x/2$	$\mathcal{T}_0/2$	4	$L_x/2$	$\mathcal{T}_0/2$	2	$2L_x/2$	$2\mathcal{T}_0/2$	2	$2L_x/2$	$2\mathcal{T}_0/2$
$[Ts]_3$	⋮	⋮	⋮	⋮	⋮	⋮	1	$2L_x/3$				
$[Tt]_3$	⋮	⋮	⋮	⋮	⋮	⋮	2	$2L_x/3$	$2\mathcal{T}_0/3$	2	$2L_x/3$	$2\mathcal{T}_0/3$
⋮	⋮	⋮	⋮	⋮	⋮	⋮	⋮	⋮	⋮	⋮	⋮	⋮

Different from a purely two-dimensional model such as a square system in which each particle can collide with any other particle, in the quasi-one-dimensional model a separation between the stepwise region and the smoothly changing region of the Lyapunov spectrum is not clear. In Ref. [19], this point was explained as being caused by the fact that particles interact only with the two nearest-neighbor particles, whereas in the purely two-dimensional low-density systems particles can interact with more than two particles.

In this paper, we considered the quasi-one-dimensional systems only. However, there should be many other interesting situations in which we can investigate structures of the Lyapunov spectrum and the Lyapunov vectors. For example, we may investigate the effect of the rotational invariance of the system on such structures by considering a two-dimensional system with a circle shape. One might also investigate the system in which the orbit is not deterministic anymore, in order to know whether the deterministic orbit plays an important role in the stepwise structure of the Lyapunov spectrum or not. It may also be important to investigate the dependence of the stepwise structures of the Lyapunov spectra on the spatial dimension of the system, for example, to investigate any structure of the Lyapunov spectra for purely one- or three-dimensional many-particle systems. (Note that the quasi-one-dimensional systems considered in this paper are still two-dimensional systems in the sense of the phase space dimension.) These problems remain to be investigated in the future.

Finally, we wish to emphasize the important conclusions of this work.

(1) For the system considered here, the quasi-one-dimensional model with various combinations of periodic and hard-wall boundary conditions, we can interpret all of the Lyapunov modes as either due to spatial translational invariance $[Ts]$ or due to time translational invariance $[Tt]$. All modes are transverse, and no longitudinal modes have been required [17] to categorize the Lyapunov modes. However, this does not preclude the existence of longitudinal modes.

(2) It is necessary to include the time translational invariance to obtain Lyapunov modes for the purely hard-wall system, as the system does not have any spatial translational invariance but still exhibits a clear stepwise structure. Therefore, we conclude that spatial translational invariance alone is not sufficient to explain the Lyapunov modes [20].

ACKNOWLEDGMENTS

The authors wish to thank C. P. Dettmann and H. A. Posch for valuable comments to this work. One of the authors (T.T.) acknowledges information on presentations of figures by T. Yanagisawa. We are grateful for financial support for this work from the Australian Research Council.

[1] P. Gaspard, *Chaos, Scattering and Statistical Mechanics* (Cambridge University Press, Cambridge, 1998).

[2] J.R. Dorfman, *An Introduction to Chaos in Nonequilibrium Statistical Mechanics* (Cambridge University Press, Cambridge, 1999).

[3] Ch. Dellago, H.A. Posch, and W.G. Hoover, Phys. Rev. E **53**, 1485 (1996).

[4] Lj. Milanović, H.A. Posch, and Wm.G. Hoover, Mol. Phys. **95**, 281 (1998).

[5] H.A. Posch and R. Hirschl, in *Hard Ball Systems and the Lor-*

entz Gas, edited by D. Szász (Springer, Berlin, 2000), p. 279.
[6] S. McNamara and M. Mareschal, Phys. Rev. E **63**, 061306 (2001).
[7] Lj. Milanović and H.A. Posch, J. Mol. Liq. **96-97**, 221 (2002).
[8] K. Kaneko, Physica D **23**, 436 (1986).
[9] K. Ikeda and K. Matsumoto, J. Stat. Phys. **44**, 955 (1986).
[10] I. Goldhirsch, P.-L. Sulem, and S.A. Orszag, Physica D **27**, 311 (1987).
[11] R. Livi and S. Ruffo, in *Nonlinear Dynamics*, edited by G. Turchetti (World Scientific, Singapore, 1989), p. 220.
[12] M. Falcioni, U.M.B. Marconi, and A. Vulpiani, Phys. Rev. A **44**, 2263 (1991).
[13] T. Konishi and K. Kaneko, J. Phys. A **25**, 6283 (1992).
[14] M. Yamada and K. Ohkitani, Phys. Rev. E **57**, R6257 (1998).
[15] A. Pikovsky and A. Politi, Phys. Rev. E **63**, 036207 (2001).
[16] Y.Y. Yamaguchi and T. Iwai, Phys. Rev. E **64**, 066206 (2001).
[17] C. Forster, H.A. Posch, R. Hirschl, and W.G. Hoover, e-print nlin.CD/0211047.
[18] T. Taniguchi, C.P. Dettmann, and G.P. Morriss, J. Stat. Phys. **109**, 747 (2002).
[19] T. Taniguchi and G.P. Morriss, Phys. Rev. E **65**, 056202 (2002).
[20] J.-P. Eckmann and O. Gat, J. Stat. Phys. **98**, 775 (2000).
[21] S. McNamara and M. Mareschal, Phys. Rev. E **64**, 051103 (2001).
[22] A. de Wijn and H. van Beijeren, in International Workshop and Seminar on Microscopic Chaos and Transport in Many-Particle Systems Max-Planck-Institut für Physik komplexer Systeme, Dresden, Germany, 2002, unpublished.
[23] The density ρ used in this paper is the reduced density, namely, the ratio of the area ($N\pi R^2$) occupied by hard disks to the total area (L_xL_y). This should be distinguished from another density called the particle number density which is defined by $\tilde{\rho}\equiv N(2R)^2/(L_xL_y)$ in our notation. The particle number density has been used in some works on the subject of Lyapunov spectrum and mode with $R=1/2$ [7,17]. These two kinds of density are simply related by $\rho=\pi\tilde{\rho}/4$.
[24] V.I. Arnold, *Mathematical Methods of Classical Mechanics*, 2nd ed. (Springer-Verlag, Berlin, 1989).
[25] G. Benettin, L. Galgani, and J.-M. Strelcyn, Phys. Rev. A **14**, 2338 (1976).
[26] I. Shimada and T. Nagashima, Prog. Theor. Phys. **61**, 1605 (1979).
[27] G. Benettin, L. Galgani, A. Giorgilli, and J.-M. Strelcyn, Meccanica **15**, 9 (1980).
[28] G. Benettin, L. Galgani, A. Giorgilli, and J.-M. Strelcyn, Meccanica **15**, 21 (1980).
[29] H. van Beijeren, A. Latz, and J.R. Dorfman, Phys. Rev. E **57**, 4077 (1998).